Developing Targeting Techniques for the Advancement of *In Vivo* Gene Therapies

Kurt Berckmueller

A dissertation submitted in partial fulfillment of the Degree of

Doctor of Philosophy

University of Washington

2023

Reading Committee:

Hans-Peter Kiem, Chair

Brandon Hadland

Barry Stoddard

Program Authorized to Offer Degree:

Molecular Medicine and Mechanisms of Disease

University of Washington

Developing Targeting Techniques for the Advancement of *In Vivo* Gene Therapies

Kurt Berckmueller

Chair of Supervisory Committee:

Hans-Peter Kiem

Department of Medicine and Pathology

Abstract:

Hematopoietic Stem Cell (HSC) gene therapy is a promising route to curing patients with a variety of hematologic diseases and disorders. HSC gene therapy is currently performed *ex vivo* and requires rare cleanroom infrastructure, which is a significant obstacle to patients in resource impoverished areas. Application of gene therapy agents directly in the patient (*in vivo)* would overcome this bottleneck. We have previously identified the $CD34^{+}CD90^{+}$ subset to be exclusively responsible for short- and long-term engraftment. However, purification and enrichment of this subset is laborious and expensive. HSC-specific delivery agents for the direct modification of rare HSCs are currently lacking. Here, we developed novel targeted viral vectors to specifically transduce CD90-expressing HSCs. Anti-CD90 single chain variable fragments (scFvs) were engineered onto measles- and VSVG-pseudotyped lentiviral vectors that were knocked out for native targeting. We further developed a custom hydrodynamic titration methodology to assess the loading of surface-engineered capsids, measure antigen recognition of the scFv, and predict the performance on cells. Engineered vectors formed with minimal impairment in the functional titer maintained their ability to fuse with the target cells and showed highly specific recognition of CD90 on cells *ex vivo*. Most importantly, targeted vectors selectively transduced human HSCs with secondary colony-forming potential. However, agents recognizing only a single marker on

target cells are often insufficient due to epitope sharing in between on- and off-target tissues. The Baker Lab previously designed a system of protein switches known as Co-LOCKR, which enable the specific recognition of two antigens simultaneously. Co-LOCKR targeted CAR T cells highly specifically killed tumor cells in vitro with virtually no off-target effects. Therefore, we further designed and evaluated Co-LOCKR-targeted viral vectors for ex vivo as well as in vivo applicability and comprehensively evaluated the on-target specificity in a murine tumor model. Together this work lays a foundation and provides a robust toolset for the exploration of *in vivo* gene therapies.

Contents

Acknowledgements:

The Thesis and the work contained within it would not have been finished without the extensive assistance of friends, mentors, and family.

I would like to thank the Kiem lab as a gestalt, and in particular Hans-Peter Kiem and Stefan Radtke for their extensive mentorship and assistance and for dragging me, sometimes with great effort and always kindly, across this line in my education.

My committee as well, has been an excellent bellwether for my progress and has been quite helpful in their critiques and encouragements of my work.

Graduate school is not always easy, but M3D and the camaraderie and mentorship I have received there from both fellow students as well as administrators have made the entire process as smooth as one could hope.

It almost goes without saying, but the mountains in the Cascades and Olympics have been a place of solitude and peace that I can go to whenever things are tough. Thank you, mountains.

The world is a big place, it gets lonely at times, we can't all carry our Sisyphean boulder alone. I have many friends and family, both in the pacific northwest and far away, with whom I could not imagine life being worth living. From hiking with them to long phone calls to playing dungeons and dragons to

Christmas at home with the family, they give that little je ne sais quoi that makes getting out of bed each morning worth it.

Introduction:

As medicine and public health increasingly can provide therapeutic options for diseases caused by environmental factors, heritable genetic diseases continue to increase in their prominence of medical focus. The ever-advancing ability to edit and change the DNA of cells has brought genomic medicine to the forefront of clinical imagination[1]. Through either implanting entirely new genes to treat autosomal recessive disorders or gene editing to correct hereditary genetic mutations with adverse pathologies, gene editing reagents hold immense promise[2]. With the advent of ever more precise gene editing reagents such as base editors, the possibilities are ever expanding[3].

The current gold standard treatment of many hematological diseases and disorders such as sickle cell disease (SCD) and certain other malignancies is an allogenic hematopoietic stem cell transplant (HSCT)[4, 5]. This has therapeutic benefits, but few patients have HLA matched donors and transplants with other donors can cause significant toxicities such as graft versus host disease, rejection, and death[6]. Autologous transplantation of gene corrected patient cells is a promising way to overcome the issues listed above, and has had success in treatment of Sickle Cell Disease(SCD) and Fanconi Anemia, however substantial usage of expensive clinical grade gene-modifying reagents, low targeting of true HSCs and potential off target effects on non-HSCs represents a large hurdle to overcome[7-20]. In addition, all current HSC gene therapies are performed *ex vivo*, which necessitates extensive medical infrastructure such as cleanrooms and prevents this treatment from being accessible in resource deprived areas of the

globe. Moving towards *in vivo* gene therapies represents a way to provide these amazing therapeutic opportunities to people in a more equitable manner.

One of the key areas of challenge in the HSC gene therapy field is the matter of targeting. This is crucial for a variety of reasons, from ensure the gene modifying vehicles can home in on the cell types of interest but also to avoid potentially deleterious off target effects. A great variety of adenovirus-, adeno-associated virus (AAV)-, as well as nanoparticle (NP)-mediated *in vivo* delivery approaches are currently tested for various non-hematological as well as hematological diseases and disorders[21, 22]. HSC therapy is performed primarily on CD34+ cells, a heterogenous mixture of overwhelmingly lineage committed progenitor cells and very few true self-renewing stem cells[23]. Attempts to design CD34 target vectors for HSC gene therapy have been less successful due to lack of phagocytosis[24]. Other markers of HSCs, including CD117 and CD133, have been considered as strategies to engage in targeted gene therapies[25, 26]. However, $CD117^+$ as well as $CD133^+$ HSPCs contain various erythro-myeloid and lympho-myeloid progenitors still bearing the risk for off-target effects[27, 28]. The current inability to reliably target gene-modifying agents specifically to these rare multipotent HSCs significantly reduces the efficiency of existing approaches and at the same time increases the risk for secondary diseases due to the modification of non-HSCs[7-12, 29].

CD90, or Thy-1 is a heavily glycosylated surface protein that is thought to play a role in cell to cell adhesion[30]. It plays a role in the life cycle of several viruses, being critical for the integration of Cytomegalovirus (CMV) via micropinocytosis into CD34+ HSCs as well as participating in HIV infection through manners thus far not mechanistically understood[31, 32]. The Kiem Lab has previously shown that the CD90+CD34+ subset of HSC's is exclusively responsible for rapid recovery onset, robust long-term multilineage engraftment, and entire reconstitution of the bone marrow (BM) stem cell compartment in the autologous nonhuman primate (NHP) and xenograft (human/NHP) transplant setting[25, 33, 34]. $CD34^+CD90^+$ cells are almost entirely depleted for phenotypically and transcriptionally committed

progenitor cells and demonstrate the greatest enrichment of multipotent HSCs with only a single marker in comparison to currently proposed alternative approaches using CD133, or CD38[33, 35-37]. Purification and direct gene modification of the HSC-enriched $CD34^{+}CD90^{+}$ phenotype significantly increased the efficiency of lentivirus (LV)-mediated gene transfer *ex vivo* and led to greater *in vivo* engraftment of gene-modified human cells in NSG mouse xenograft transplant[25]. These combined facts indicated to us that attempting to target CD90 could be a viable strategy for gene therapy of a more refined HSC population that has precedent in nature.

However, targeting CD90 alone may still pose difficulties for *in vivo* gene therapies. CD90 is present on other cells within the bone marrow compartment such as mesenchymal stem cells, as well as other cell types like thymocytes throughout the body, representing possibilities of off target events occurring[38, 39]. Other single markers of interest in HSC research such as CD133 or CD117 are frequently present on other cell types as well. One method of reimagining targeting to avoid such undesired effects is to combine targeting moieties. The Baker lab at the University of Washington has previously shown that by using their do-novo Co-LOCKR proteins, which enable combinatorial targeting techniques, they could specifically show directed targeting of CAR-T cells against two different cancer moieties with high specificity[40, 41]. We hoped that these highly encouraging results could also be applied towards targeting gene modifying reagents to HSC's, utilizing combinations of targeting markers that would avoid almost all off target possibilities.

In the following studies, we designed and characterized an anti-CD90 scFv, engineered it onto the surface of a modified lentivirus with, and comprehensively tested this virus's ability to target cells of interest. We additionally partnered with the Baker lab to test their Co-LOCKR protein system which had previously been used for CAR T cell targeting and tested its ability to be used for targeting viruses to transduce specific cell types displaying two markers.

Chapter 1 CD90 Targeting:

Introduction:

Currently existing gene therapy approaches modify $CD34^+$ hematopoietic stem and progenitor cells (HSPCs), a heterogeneous population that contains less than 1% HSCs with long-term multilineage engraftment potential [23]. Consequently, massive use of expensive reagents, potential off target effects in non-HSCs, and low on-target efficiency currently impact the feasibility of HSC gene therapy[6]. In addition, current gene therapy approaches rely on the modification of HSCs outside the patient's body (*ex vivo*) and require highly specialized facilities like bone marrow transplantation severely limiting the accessibility of this treatment option. Injection of gene therapy agents and modification of HSCs directly in the patient (*in vivo*) would overcome all these limitations. However, a major obstacle to perform gene therapy *in vivo* is the lack of HSC-targeted gene therapy agents to deliver the therapeutic cargo and avoid off-target effects highly specifically.

Targeted delivery depends on the uptake of the vector after attaching to the cell/antigen, which could not be achieved with CD34-targeted HSC gene therapy vectors [24]. Therefore, alternative markers of HSCs such as CD117 and CD133 are being considered [25, 42]. However, $CD117^+$/$CD133^+$ cells contain various erythro-myeloid and lympho-myeloid progenitors [43, 44] that bear the risk for unwanted off-target effects. Lastly, CD133 as well as CD117 are readily expressed on cells in the lung, liver, and reproductive organs *(proteinatlas.org*), likely leading to

rapid clearance of CD133/CD117-targeted vectors as well as unknown side-effects when applied *in vivo*.

Previous work in the lab has shown that the $CD90^+$ subset of $CD34^+$ HSPCs is exclusively responsible for rapid recovery onset, robust long-term multilineage engraftment, and entire reconstitution of the bone marrow (BM) stem cell compartment [25, 34, 45]. Furthermore, $CD34^+CD90^+$ cells are almost entirely depleted for phenotypically, transcriptionally, and functionally committed progenitor cells [25, 35-37]. Isolation and direct targeting of this HSC-enriched subset from mobilized human apheresis products *ex vivo* significantly increased lentivirus-mediated gene transfer without impacting the cells long-term multilineage engraftment potential (2).

To enable highly specific targeting of $CD90^+$ HSCs, we here designed CD90-targeted viral vectors engineering an anti-CD90 single chain variable fragment (scFv) onto measles-pseudotyped lentiviral vectors. CD90-targeted viral vectors were further knocked out for their native targeting to optimize on-target specificity. Lastly, we developed hydrodynamics-based methodology to easily and reliably titrate and quality control our surface-engineered viral vectors.

Results:

CD90 scFv design, modification, and validation

To generate HSC-targeted viral vectors for gene therapy, we initially designed and computationally validated an scFv recognizing CD90. Sequences for the scFv design were extracted from the hybridoma cell line producing the CD90 antibody clone 5E10 [46, 47]. Briefly,

mRNA was extracted from the cell line, reverse transcribed, and primers designed to sequence the cDNA fragments encoding for the variant light and heavy regions (**Figure 1A**). To determine the framework and complementary defining regions of the antibody, sequences were annotated using IMGT [48, 49]. Next, scFv's were designed linking the light- and heavy-chain sequences using the commonly used 3x(GGGGS) hinge (**Figure 1B**). Finally, to predict the binding ability of our anti-CD90 scFv with the extracellular domain of CD90, interactions were modelled using Swissdock [50] (**Figure 1C**). Although bioinformatics predicted successful binding, no expression of the anti-CD90 scFv could be achieved (data not shown). Comprehensive comparison of our sequences with the database revealed two cysteine residues (position 31 and 59) that were not found in any other reference and were not predicted to form disulfate bonds running SAbPred modelling [51]. Cysteines were therefore exchanged (position 31 Tyrosine [Y], position 59 Arginine [R]) to match the reference sequences. In addition, the linker was exchanged to an alternate linker sequence (GSDSN AGHAS AGNTS) [52] to enable easier production and sequencing of variants.

Design, production, and hydrodynamic titration of CD90-targeted measles-pseudotyped viral vectors

Measles-pseudotyped lentiviral vectors efficiently transduce a wide variety of cell types recognizing the broadly expressed cell surface antigens CD46 and CD150 [53, 54]. Here we stepwise developed the measles-envelope to remove the native targeting and instead exclusively recognize CD90 as previously described for other target cells [52]. In addition to the wildtype envelope (Variant H1: WT), three variants of the measles envelope were generated (**Figure 2A**). To remove its ability to target CD46/150 and thus creating a virus that should not be able to elicit

fusion and transduce cells [55], four modifications were introduced to the amino acid sequence of the measles glycoprotein (Variant H2: KO). We next created a variant that can detect CD46, CD150 and CD90 inserting the CD90 scFv at the end of the glycoprotein (Variant H3: WT/CD90). Finally, the CD46/CD150 KO and CD90 recognition was combined leading to a variant that should only bind and fuse on CD90-expressing cells (Variant H4: KO/CD90).

Due to the inability of the KO variants to be titrated on standard cell lines such as HT1080 (**Figure 2B**), we further developed methodology using hydrodynamics combined with fluorescence to determine the number of total as well as mRNA filled viral particles. Size and number of viral particles were determined using the ZetaView®, a Nanoparticle Tracking Analysis (NTA) instrument for measuring particle size, zeta potential, concentration, and fluorescence (**Figure 2C**). Regardless of the modifications and addition of the CD90 scFv, all four envelope variants equally produced viral particles (**Figure 2D**). Successful loading of viral capsids and loading efficiency was determined staining the particles with SYBR II. The number of mRNA-loaded viral particles was highly variable across batches (**Figure 2E**). However, the loading efficiency of viral particles (frequency of mRNA-loaded particles within total particles) was very consistent averaging at 10 to 20 % with no obvious differences due to the modification made (**Figure 2F**).

CD90 scFv on viral vectors bind CD90 protein:

To ensure the ability of CD90-targeted viral vectors to recognize CD90 antigen, we designed a custom assay using NTA. The extracellular domain of CD90 was fused with the fluorochrome mCherry (CD90-mCh) and the fusionprotein produced with the Daedalus system

[56]. The quality of the CD90-mCh fusion protein was confirmed demonstrating its interaction with anti-CD90 Fabs from the hybridoma cell line using size exclusion chromatograph (SEC) using an A200 column run in PBS buffer. Each protein exhibited a single peak at the expected molecular weight (MW) (**Figure 3A**). Fab binding to CD90-mCh was confirmed by the shift of the elution peak to a larger MW species, and by SDS-PAGE of the peak showing presence of both proteins.

Next, we measured the size of our vector variants in the presence and absence of the CD90-mCh protein (**Figure 3B**). All four vectors were very similar in size (range 110-130nm) regardless of the modificaitons made measuring the scattered light (**Figure 3C,** top row). Adding SYBR II to stain only RNA-loaded particles and observing the fluorescence in the 500nm filter, particles appear slighlty larger across all four variants and a boader size range due to variability in RNA loading (**Figure 3C,** middle row). Finally, vectors incubated with CD90-mCh protein were measured (**Figure 3C,** bottom row). Due to the background noise of unbound protein in the 600nm filter, measurements were performed in the 500nm filter focusing only on RNA-loaded particles. As expected, CD90-decorated viral variants H3 and H4 with CD90-mCh formed new peaks at 300nm indicating formation of a complex. Only a minor change in size was seen for variant H1 and H2 lacking the CD90 scFv due to additional background noise signal from the CD90-mCh protein.

In summary, we were able to successfully engineer an anti-CD90 scFv onto the Measles envelope without imparing the vector production and maintaining viral titers. Most importanlty, anti-CD90 scFvs on the viral capsid are fully functional and able to recognize CD90 antigen in our custom hydrodynamic readout confirming CD90 specificity of the scFv.

Targeted viral vectors transduce CD90-expressing Jurkat cells and human HSCs:

The Measles envelope has been extensively modified and previous attempts to use similar systems to specifically transduce $CD34^+$ cells failed due to the lack of fusion with the target cells [24]. Consequently, we next assessed our CD90-targeted viral vectors for fusion and transduction ability. For the initial tests, CD90-expressing Jurkat cells were used and incubated with all four viral variants. Jurkat cells were kept in culture for 5-7 days to guarantee stable integration of the transgene and wash out transiently delivered florescent protein sticking on the viral particles.

Determined by flow-cytometry, we observed robust transduction of Jurkat cells with variant H1 (WT, 15.3±7.4%, n=4). Relative to variant H1, knock-out of CD46 and CD150 recognition reduced the ability of variant H2 to transduce Jurkat cells by 81.6±13.4% (**Figure 4A**). Addition of the CD90 scFv on the H WT virus (variant H3) had no impact on the transduction ability in comparison to the WT variant H1. Finally, variant H4 (KO/CD90) regained transduction capability over variant H2 (KO) reaching on average 44.8±17.9% transduction efficiency. We further evaluated the reliability of hydrodynamic titers determined with NTA for variant H1 (**Figure 4B**). Exceedingly high correlation (R^2=0.9315) was found in between the number of mRNA-loaded particles and the number of transduced cells.

Next, we transduced human GCSF-mobilized $CD34^+$ cells with variant H1 and H4 vectors to analyze the targeting efficiency of the $CD34^+$CD90+ subset (**Figure 4C**). Due to the internalization/blocking and resulting inability to detect CD90 surface expression after exposure to the variant 4 virus by flow-cytometry, mScarlet expressing $CD34^+$ cells from both conditions were FACS-purified and introduced into colony-forming cell (CFC) assays to functionally

determine difference in the targeting of both viruses. No differences in the total colony-formation were seen comparing the WT and CD90-targeted virus in primary CFCs, whereas more colonies were found in secondary CFCs when the targeted virus was used indicating selective transduction of more primitive human HSPCs with enhanced proliferation potential with variant 4. Colonies in secondary CFC assays from variant H4-transduced cells contained more total cells as well as a greater number of stably mScarlet-expressing cells confirming greater proliferation and expansion potential of cells transduced with the CD90-targeted virus.

This data confirms that CD90-targeted viral vectors are capable to recognized CD90 antigen on the surface of Jurkat cells as well as human HSCs and effectively fuse with the cells. Furthermore, hydrodynamic titers were highly predictable for the transduction efficiency confirming accuracy and validity of our new titration methodology for surface-engineered viral vectors.

On-target efficiency of CD90-targeted viral vectors

To evaluate the on- and off-target activity of our CD90-targeted Measles- as well as VSVG-pseudotyped viral vectors, we performed co-culture experiments mixing CD90-lacking (off-target) and CD90-expressing (on-target) suspension cell lines. Raji cells, human B lymphoblastoid cells, do present very low levels of CD90 protein on the cell surface (off-target), whereas Jurkat cells, immortalized human T lymphocytes, express CD90 protein at high levels (on-target) (**Figure 5A**). GFP-transduced Jurkat cells and GFP^- Raji cells were mixed and exposed to Measles and VSVG

variants 1 and 4 in a serum-free, transduction enhancer-free, suspension culture system, and mScarlet expression flow-cytometrically determined on day 3-5 post-transduction (**Figure 5B**). When the variant H1/V1 (WT) virus was used, mScarlet expression was seen for Raji as well as Jurkat cells by flowcytometry. However, when the cell mix was exposed to variant H4/V4 (KO/CD90), a strong preference of mScarlet signal was seen in the $CD90^{+}$ Jurkat cells (on-target) and only minimal transduction in the $CD90^{low/-}$ Raji cells (off-target) (**Figure 5B**). To quantify the on-target specificity, we calculated the ratio of $mScarlet^{+}GFP^{-}$ cells within total GFP^{-} Raji to $mScarlet^{+}GFP^{+}$ cells within total GFP^{+} Jurkat cells (**Figure 5C**). For both virus types, the CD90-targeted variant 4 showed significantly higher on-target specificity in comparison to the variant 1 (WT) confirm CD90-mediated target specificity.

DISCUSSION

Here we demonstrate the successful design of CD90-targeted Measles- and VSVG-based viral vectors equipping viral capsids with a novel anti-CD90 scFv. Surface engineering did neither impact titers, binding, nor fusion of viral vectors to CD90-expressing cell lines and primary human HSCs. Most importantly, targeted vectors demonstrated enhanced on-target specificity in mixed cultures of cell lines as well as for human HSCs within bulk $CD34^+$ HSPCs *ex vivo*. We further describe novel NTA-based methods to reliably quality control surface engineered viral vectors measuring their size, loading-efficiency, and targeting functionality. Hydrodynamic titration of engineered vectors is highly reproducible and predictive of the transduction efficiency providing a dependable surrogate to functional readouts on cell lines not applicable to surface engineered vectors.

The development of targeted gene therapy agents has been extraordinarily successful for non-hematological diseases [22, 57-60]. Previous work has shown that by conjugating antibodies or scFv's to the surface of nanoparticles (NPs) and viruses, one can reliably target cells of interest [24, 42, 54, 57, 60-66]. Targeted delivery however depends on the uptake of the vector after attaching to the cell/antigen, which could not be achieved with CD34-targeted HSC gene therapy vectors [24]. Here we designed CD90-targeted viral vectors that successfully fused and transduced CD90-expressing cell lines as well as $CD34^+CD90^+$ HSCs with secondary colony-forming potential. Although the exact mechanism of CD90-mediated cellular uptake is not known, cytomegalovirus (CMV) and Human Immunodeficiency Virus (HIV) use CD90 as a crucial part of their cellular entry process [31, 32, 67]. CMV entry was interrupted when CD90 was either blocked with an antibody or downregulated using an siRNA approach [31]. In addition, liposomes

conjugated with anti-CD90 antibodies have been shown to be capable of binding and internalizing through the CD90 antigen on liver cancer cells, demonstrating efficient uptake of CD90-targeted lipid nanoparticles (LNPs) also *in vivo* [68]. Our viral vectors have been genetically modified to lose their native binding (LDLR for VSVG; CD46 and CD150 for Measles), but their ability to fuse with the target cell remains intact. The CD90 scFv is therefore likely acting as a binder, whereas cellular entry remains to be dependent on viral capsid. More in-depth studies will be required to determine whether CD90 is actively involved in the uptake, which pathways are triggered, and whether this system can also be used completely independent from viral fusion proteins. Regardless of the exact pathways involved, CD90 protein was internalized on primary human HSCs without any obvious impact on the cell's proliferation and differentiation potential. Follow-up work will be needed to evaluate the recycling and re-expression of CD90 protein on the cell surface after CD90-mediated viral entry to ensure that the long-term multilineage engraftment of HSCs is warranted.

A major bottleneck for the development of surface engineered viral vectors for HSC gene therapy is the inability to quickly and reliably quality control the vectors before use. Genetically engineered viral vectors lost their native binding and functional titration methods on HEK293T or HT1080 cell lines are not possible. In addition, validation of antigen/target recognition is needed to ensure that surface-engineered viral vectors are functional and targeting ligands have been successfully integrated into the capsid. To close this gap, we here developed novel methodology to titrate and quality control viral vectors using nanoparticle tracking analysis (NTA). NTA allows for the efficient and reliable quantification of viral vector concentration, size, and mRNA loading. Most importantly, hydrodynamic viral titers correlated with the transduction efficiency on cell

lines for wildtype variants providing a surrogate method for the traditional titration on cell lines or other qPCR-based strategies. NTA was further used to demonstrate successful antigen recognition of targeted vectors. Custom-designed fluorochrome-conjugated CD90 protein was bound by the scFv-decorated Measles-pseudotyped viral vectors resulting in a size increase measured by NTA and confirming fully functional antigen recognition when the targeting ligand is presented on the virus. The measurement of these parameters is almost instant and does provide a new alternative to traditional titration methods of wildtype, novel surface-engineered viral vectors, as well as virus-like particles. As viral vectors often undergo freezing and thawing, quality control and quantification of viral particles can even be performed right before applying them to the cells or injecting them *in vivo*, providing an opportunity to adjust and carefully control viral titers in real-time.

A major advantage of our CD90-targeted viral vectors is the ability to incorporate them instantaneously into already existing *ex vivo* gene therapy pipelines focusing on the gene-modification of $CD34^+$ HSPCs. Further purification of the $CD90^+$ subset for direct targeting and to enhance the transduction efficiency [25] would potentially no longer be needed to transduce long-term engrafting HSCs and likely require even lower viral titers reducing the overall costs. Even the purification of $CD34^+$ cells from the leukapheresis products may no longer be necessary proving a novel vector to realize closed-system vein-to-vein applications with the transduction of cells in bags and immediate infusion of the transduced cells back into the patient[69]. Finally, direct intravenous or intraosseous injection of the HSC-targeted viral vectors would be warranted further simplifying HSC gene therapy, proving full portability, and consequently better accessibility. However, before such targeted vectors can enter the clinical routine,

comprehensive *in vivo* studies in humanized mice as well as large animals such as the nonhuman primate will be needed to test the on-target specificity, determine the half-life/pharmacokinetics in circulation, evaluate serum susceptibility, and analyze potential off-target effects.

Especially for in vivo applications, various avenues need to be explored to provide best targeting, highest efficiency, and least off target effects. Adaptation of the targeting system using Cocal-pseudotyped lentiviral vectors which are less susceptible to serum inactivation may be favorable for *in vivo* administrations [70, 71]. Furthermore, the targeting of multiple HSC-associated cell surface markers using colocalization-dependent protein switches (Co-LOCKR) protein switches may help to increase the on-target specificity [41]. Finally, adaptation of our targeting ligand for the use with non-viral delivery platforms such as polymer or lipid nanoparticles [72] as well as virus like particles [73] may enable the transient delivery of nucleases or therapeutic mRNAs and proteins without the risk of insertional mutagenesis.

Our new CD90-targeted vectors have the potential to improve already existing *ex vivo* HSC gene therapies as well as overcome current hurdles to apply gene therapy *in vivo*. The development of targeted viral vectors has the potential to increase the on-target efficiency, safety, and accessibility of HSC gene transfer for a variety of different diseases and will be a crucial step in democratizing access to gene therapies.

Chapter 1 FIGURES AND FIGURE LEGENDS

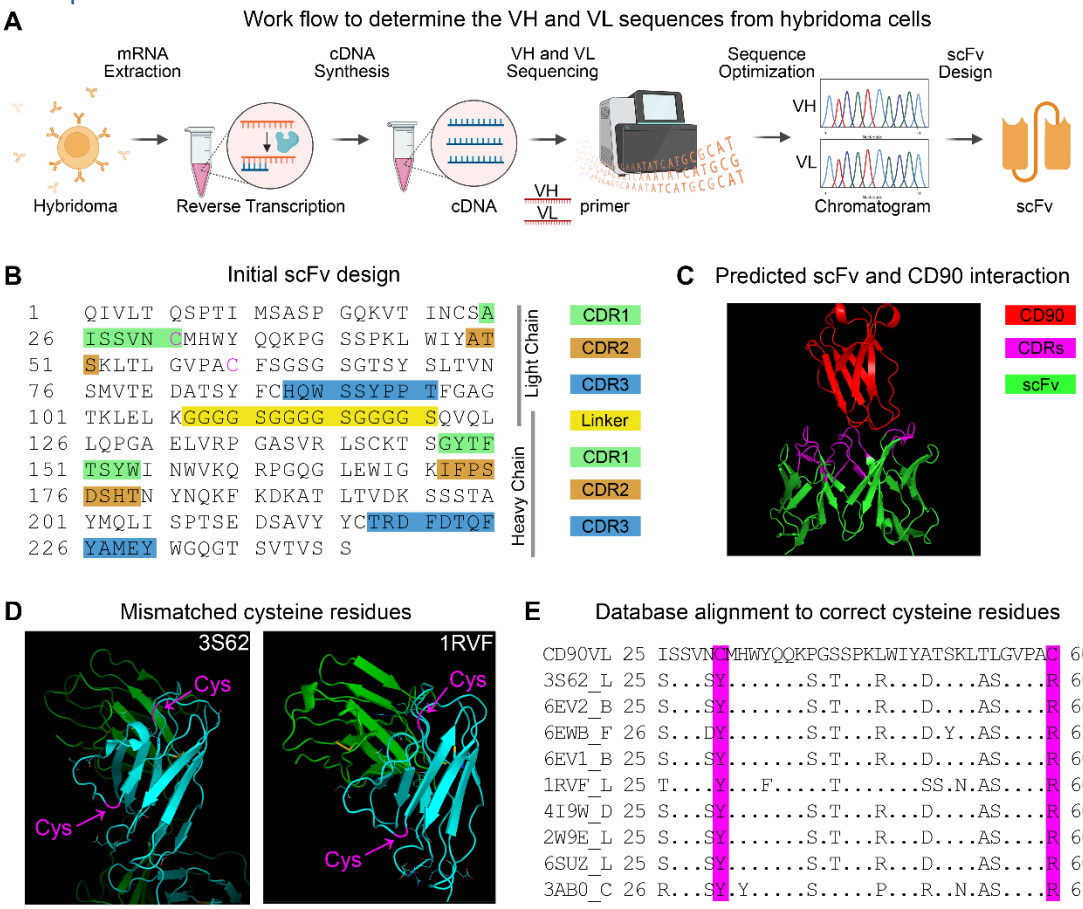

Figure 1: Design and computational validation of an anti-CD90 scFv.

(A) Workflow to determine the variant heavy (VH) and variant light (VL) sequence from the hybridoma cell line producing the CD90 antibody clone 5E10. (**B**) Amino acid sequence of the initial scFv design connecting the VL and VH chain with a 3x(GGGGS) linker[52] (yellow) sequence. Complementarity-determining regions (CDRs, color coded) for the VH and VL sequence were determined using IMGT. (**C**) Predicted interaction of CD90 (red) with the anti-CD90 scFv (green). CDRs of the scFv are highlighted in magenta. (**D**) Representative database crystal structure of 3S62 and 1RVF highlighting the regions of putative mismatched cysteines from our anti-CD90 scFv. (**E**) Sequence alignment of our anti-CD90 scFv with the reference database

for highly homologous crystal structures. Mismatched cysteines in position 31 and 59 are highlighted in magenta.

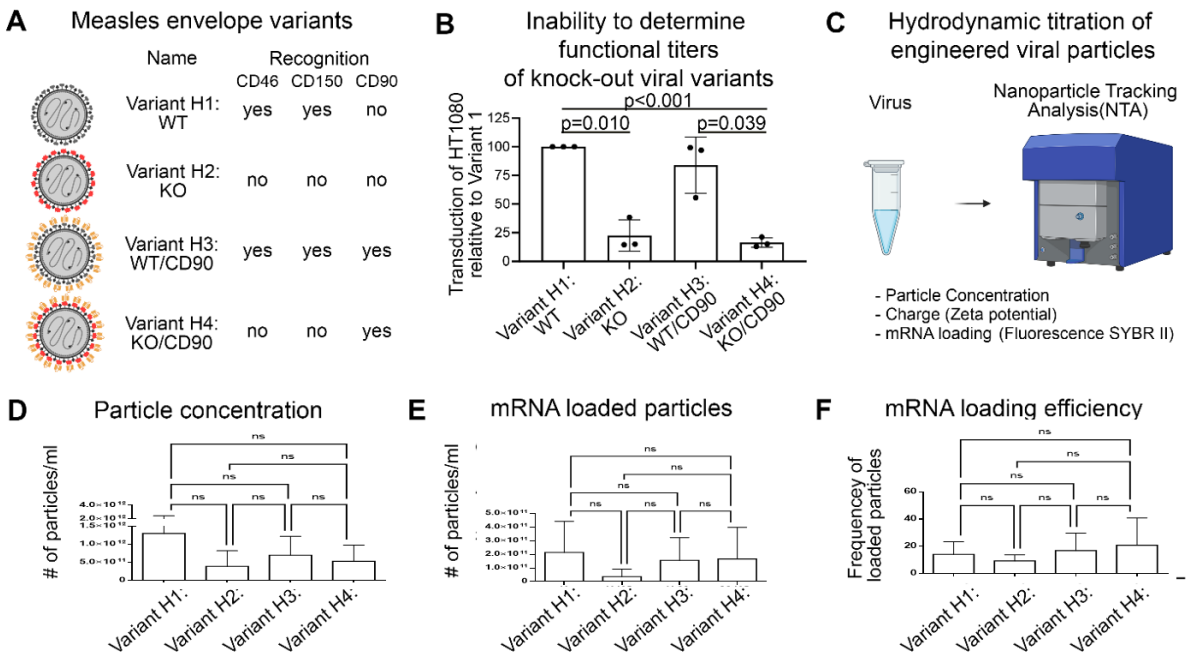

Figure 2: Design and quality control of CD90-targeted measles-pseudotyped lentiviral vectors.

(**A**) Summary of designed Measles envelopes and the expected antigen recognition. (**B**) Viral variants were evaluated on HT1080 cells demonstrating inability of the KO versions to fuse and transduce. Repeat one way ANOVA was used as a test for statistical significance. (**C**) Workflow for the hydrodynamic titration of engineered viral vectors using nanoparticle tracking analysis (NTA). (**D**) Concentration of viral particles per ml culture medium harvested. Repeat one way ANOVA was used as a test for statistical significance. (**E**) Concentration of RNA-loaded viral particles per ml culture medium measured with SYBR II. (**F**) RNA loading efficiency calculated based on values from D and E. Repeat one way ANOVA was used as a test for statistical significance.

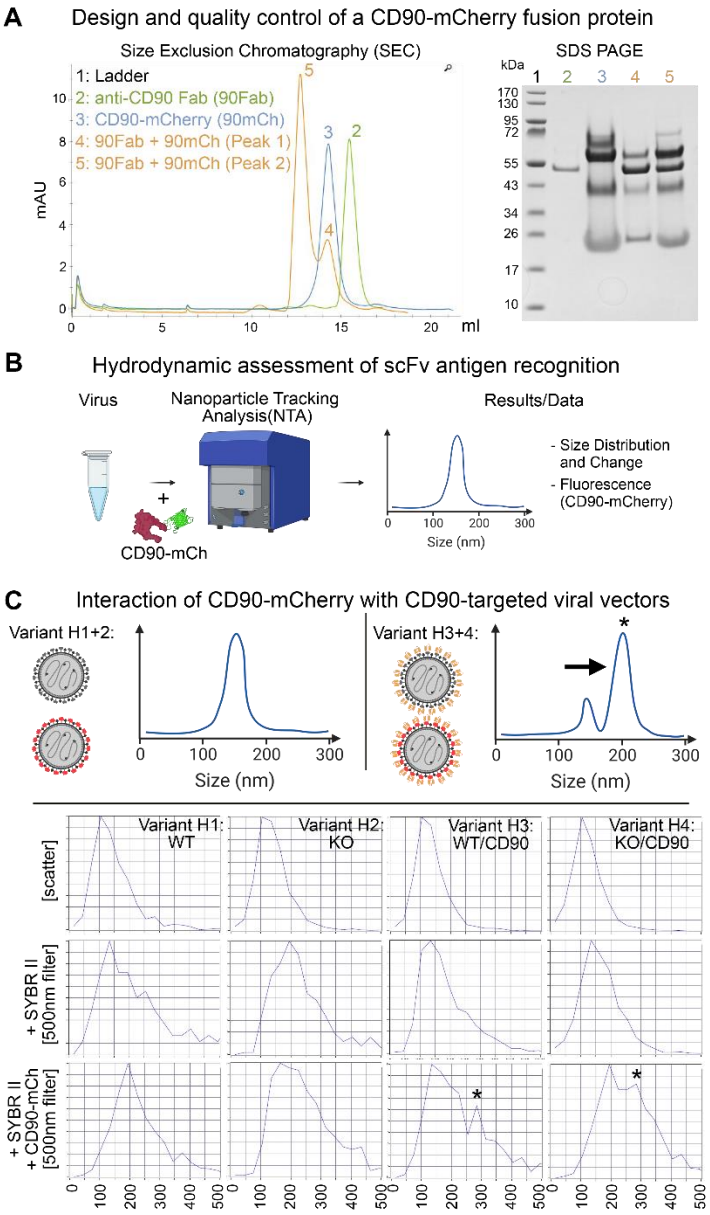

Figure 3: Assessment of antigen recognition by CD90-targeted lentiviral vectors.

(**A**) Quality control of custom produced CD90-mCherry fusion protein. CD90 Fab (1, green), CD90-mCherry fusion protein (2, blue), and a mix of CD90 Fab with CD90-mCherry were analyzed by size exclusion chomatograph (line graph). Fractions/peaks indicated with numbers were collected and content validated by SDA page (left top). (**B**) Work flow for the assessment of CD90-mCherry interaction with CD90-targeted viral vectors using nanoparticle tracking analysis

(NTA). (**C**) Size of viral particles measuring scattered light (top row). Size distribution of mRNA-loaded particles stained with SYBR II and measuring the fluorescence in the 500nm filter (middle row). SYBR II signal of mRNA-loaded viral particles co-incubated with CD90-mCh measuring the fluorescence in the 500nm filter (bottom row). Numbers in each plot indicate the average size of numbered peaks.

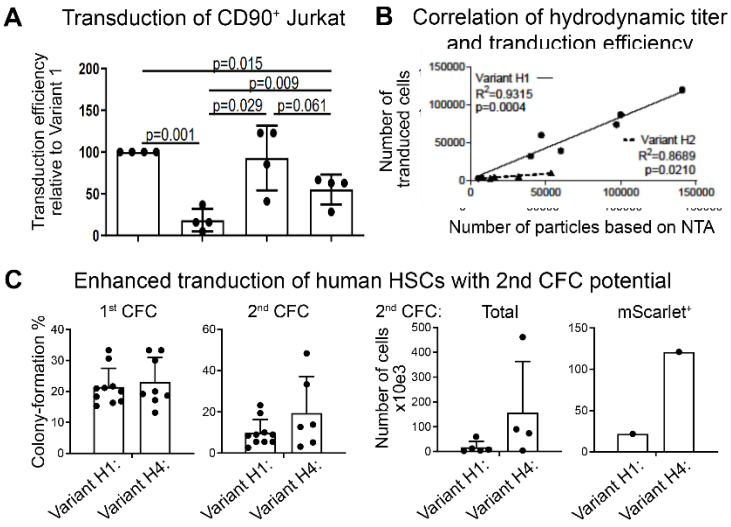

Figure 4: Selective transduction of cell lines and HSCs with CD90-targeted viral vectors.

(**A**) Flow-cytometric assessment of the transduction efficiency of Jurkat cells using all 4 vector variants. Efficiencies are visualized relative to the efficiency of variant H1 (mean±SD). (**B**) Correlation of the number of transduced cells with the number of mRNA-loaded viral particles using the WT variant H1. R^2: Spearman's rank correlation coefficient. **(C)** Functional assessment of transduced human $CD34^+$ cells in colony-forming cell (CFC) assays. mScarlet expressing $CD34^+$ cells were FACS-purified and introduced into primary (1^{st}) CFC assays (first graph). After 14 days, colonies were counted, all cells harvested, and 5% of all cells replated into secondary (2^{nd}) CFC assays (second graph). Secondary CFCs were counted after 14 days, all cells harvested, the total number of WBCs counted (third graph), and the mScarlet expression measured by flow-cytometry (fourth graph).

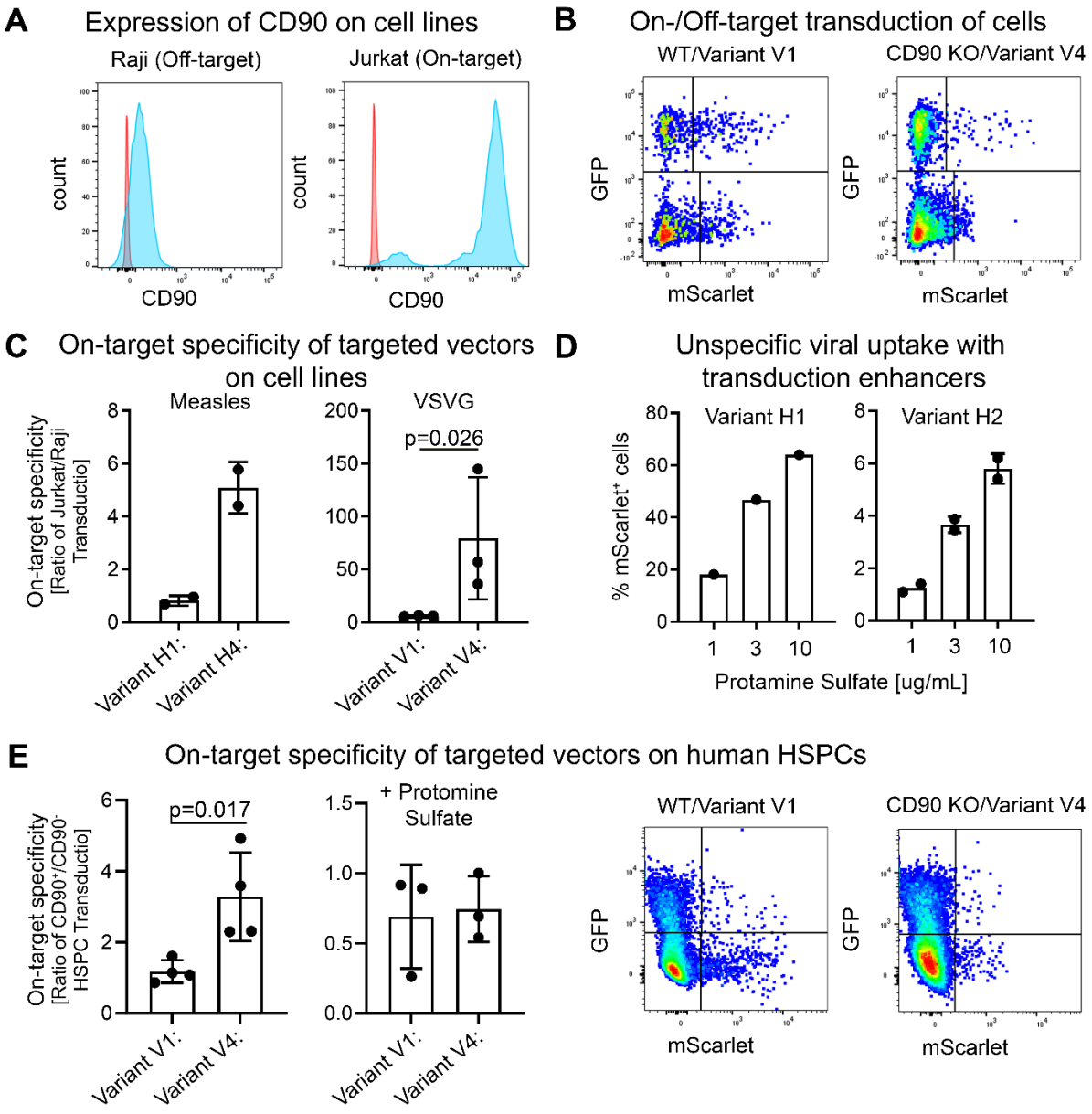

Figure 5: On-target specificity of CD90-targeted vectors.

(A) Flow-cytometric assessment of CD90 expression on Raji and Jurkat cells. (B) Flow cytometry graphs indicating off target vs on target targeting in Jurkat CD90+ cells. (**C**) Transduction efficiency of mixed cultures containing GFP^- Raji and GFP^+ Jurkat cells with

either Variant V1 or V4. (**C**) On target specificity of Measles- vector variants 1 and 4 determined by the ratio of $mScarlet^{+}GFP^{-}$ cells within total GFP^{-} Raji to $mScarlet^{+}GFP^{+}$ cells within total GFP^{+} Jurkat cells. (D) Graph showing addition of transduction enhancer, in this case Protamine Sulfate's effects on on-target vs off-target transduction in measles virus variants. (E) On and off-target effects with and without protamine sulfate with VSVG virus variants.

Supplemental Table 1:

Antigen	Vendor	Catalog Number	Clone Name	Fluorochrome	Application
CD45	BD Biosciences	560367	HI30	V450	Human HSCs
CD34	BD Biosciences	561209	563	APC	Human HSCs
CD90	BD biosciences	328124	5E10	PE-Cy7	Human HSCs, Jurkat cells Raji Cells

(B)

Supplemental Figure 1: Variant H1 WT measles

```
   1 atgaa cagag aacat cttat gattg ataga ccttа tgttt tgctg gctgt tctgt ttgtc
  61 atgtt tctga gcttg atcgg gttgc tagcc attgc aggca ttaga cttca tcggg cagcc
 121 atcta caccg cagag atcca taaaa gcctc agcac caatc tagat gtaac tactc aatcg
 181 agcat caggt caagg acgtg ctgac accac tcttc aaaat catcg gtgat gaagt gggcc
 241 tgagg acacc tcaga gattc actga cctag tgaaa ttcat ctctg acaag attaa attcc
 301 ttaat ccgga taggg agtac gactt cagag atctc acttg gtgta tcaac ccgcc agaga
 361 gaatc aaatt ggatt atgat caata ctgtg cagat gtggc tgctg aagag ctcat gaatg
 421 cattg gtgaa ctcaa ctcta ctgga gacca gaaca accaa tcagt tccta gctgt ctcaa
 481 aggga aactg ctcag ggccc actac aatca gaggt caatt ctcaa acatg tcgct gtccc
 541 tgtta gactt gtatt taggt cgagg ttaca atgtg tcatc tatag tcact atgac atccc
 601 aggga atgta tgggg gaact tacct agtgg aaaag cctaa tctga gcagc aaaag gtcag
 661 agttg tcaca actga gcatg taccg agtgt ttgaa gtagg tgtta tcaga aatcc gggtt
 721 tgggg gctcc ggtgt tccat atgac aaact atctt gagca accag tcagt aatga tctca
 781 gcaac tgtat ggtgg ctttg gggga gctca aactc gcagc ccttt gtcac gggga agatt
 841 ctatc acaat tccct atcag ggatc aggga aaggt gtcag cttcc agctc gtcaa gctag
 901 gtgtc tggaa atccc caacc gacat gcaat cctgg gtccc cttat caacg gatga tccag
 961 tgata gacag gcttt acctc tcatc tcaca gaggt gttat cgctg acaat caagc aaaat
1021 gggct gtccc gacaa cacga acaga tgaca agttg cgaat ggaga catgc ttcca acagg
1081 cgtgt aaggg taaaa tccaa gcact ctgcg agaat cccga gtggg cacca ttgaa ggata
1141 acagg attcc ttcat acggg gtctt gtctg ttgat ctgag tctga cagtt gagct taaaa
1201 tcaaa attgc ttcgg gattc gggcc attga tcaca cacgg ttcag ggatg gacct ataca
1261 aatcc aacca caaca atgtg tattg gctga ctatc ccgcc aatga agaac ctagc cttag
1321 gtgta atcaa cacat tggag tggat accga gattc aaggt tagtc cctac ctctt cactg
1381 tccca attaa ggaag caggc ggaga ctgcc atgcc ccaac atacc tacct gcgga ggtgg
1441 atggt gatgt caaac tcagt tccaa tctgg tgatt ctacc tggtc aagat ctcca atatg
1501 ttttg gcaac ctacg atact tccag ggttg aacat gctgt ggttt attac gttta cagcc
1561 caagc cgctc atttt cttac tttta tcctt ttagg ttgcc tataa agggg gtccc catcg
1621 aatta caagt ggaat gcttc acatg ggacc aaaaa ctctg gtgcc gtcac ttctg tgtgc
1681 ttgcg gactc agaat ctggt ggaca tatca ctcac tctgg gatgg tgggc atggg agtca
1741 gctgc acagt caccc gggaa gatgg aacca at
```

Sequence Nomenclature	Coloring Schema	Sequence Numbering
Hemagglutinin Endodomain		1-102
Hemagglutinin Ectodomain		103-1772

Supplemental Figure 2: Variant H2 KO measles

```
   1 atgaa cagag aacat cttat gattg ataga ccttа tgttt tgctg gctgt tctgt ttgtc
  61 atgtt tctga gcttg atcgg gttgc tagcc attgc aggca ttaga cttca tcggg cagcc
 121 atcta caccg cagag atcca taaaa gcctc agcac caatc tagat gtaac tactc aatcg
 181 agcat caggt caagg acgtg ctgac accac tcttc aaaat catcg gtgat gaagt gggcc
 241 tgagg acacc tcaga gattc actga cctag tgaaa ttcat ctctg acaag attaa attcc
 301 ttaat ccgga taggg agtac gactt cagag atctc acttg gtgta tcaac ccgcc agaga
 361 gaatc aaatt ggatt atgat caata ctgtg cagat gtggc tgctg aagag ctcat gaatg
 421 cattg gtgaa ctcaa ctcta ctgga gacca gaaca accaa tcagt tccta gctgt ctcaa
 481 aggga aactg ctcag ggccc actac aatca gaggt caatt ctcaa acatg tcgct gtccc
 541 tgtta gactt gtatt taggt cgagg ttaca atgtg tcatc tatag tcact atgac atccc
 601 aggga atgta tgggg gaact tacct agtgg aaaag cctaa tctga gcagc aaaag gtcag
 661 agttg tcaca actga gcatg taccg agtgt ttgaa gtagg tgtta tcaga aatcc gggtt
 721 tgggg gctcc ggtgt tccat atgac aaact atctt gagca accag tcagt aatga tctca
 781 gcaac tgtat ggtgg ctttg gggga gctca aactc gcagc ccttt gtcac gggga agatt
 841 ctatc acaat tccct atcag ggatc aggga aaggt gtcag cttcc agctc gtcaa gctag
 901 gtgtc tggaa atccc caacc gacat gcaat cctgg gtccc cttat caacg gatga tccag
 961 tgata gacag gcttt acctc tcatc tcaca gaggt gttat cgctg acaat caagc aaaat
1021 gggct gtccc gacaa cacga acaga tgaca agttg cgaat ggaga catgc ttcca acagg
1081 cgtgt aaggg taaaa tccaa gcact ctgcg agaat cccga gtggg cacca ttgaa ggata
1141 acagg attcc ttcat acggg gtctt gtctg ttgat ctgag tctga cagtt gagct taaaa
1201 tcaaa attgc ttcgg gattc gggcc attga tcaca cacgg ttcag ggatg gacct ataca
1261 aatcc aacca caaca atgtg tattg gctga ctatc ccgcc aatga agaac ctagc cttag
1321 gtgta atcaa cacat tggag tggat accga gattc aaggt tagtc ccgca ctctt cactg
1381 tccca attaa ggaag caggc ggaga ctgcc atgcc ccaac atacc tacct gcgga ggtgg
1441 atggt gatgt caaac tcagt tccaa tctgg tgatt ctacc tggtc aagat ctcca atatg
1501 ttttg gcaac ctacg atact tccgc agttg aacat gctgt ggttt attac gttta cagcc
1561 caagc cttga gcttt cttac tttta tcctt ttagg ttgcc tataa agggg gtccc catcg
1621 aatta caagt ggaat gcttc acatg ggacc aaaaa ctctg gtgcc gtcac ttctg tgtgc
1681 ttgcg gactc agaat ctggt ggaca tatca ctcac tctgg gatgg tgggc atggg agtca
1741 gctgc acagt cаccc gggaa gatgg aacca at
```

Sequence Nomenclature	Coloring Schema	Sequence Numbering
Hemagglutinin Endodomain		1-102
Hemagglutinin Ectodomain		103-1772
Hemagglutinin Mutations		1368-1370, 1524-1526, 1566-1571

Supplemental Figure 3: Variant H3 WT measles and targeting domain:

```
   1 atgaa cagag aacat cttat gattg ataga ccttа tgttt tgctg gctgt tctgt ttgtc
  61 atgtt tctga gcttg atcgg gttgc tagcc attgc aggca ttaga cttca tcggg cagcc
 121 atcta caccg cagag atcca taaaa gcctc agcac caatc tagat gtaac tactc aatcg
 181 agcat caggt caagg acgtg ctgac accac tcttc aaaat catcg gtgat gaagt gggcc
 241 tgagg acacc tcaga gattc actga cctag tgaaa ttcat ctctg acaag attaa attcc
 301 ttaat ccgga taggg agtac gactt cagag atctc acttg gtgta tcaac ccgcc agaga
 361 gaatc aaatt ggatt atgat caata ctgtg cagat gtggc tgctg aagag ctcat gaatg
 421 cattg gtgaa ctcaa ctcta ctgga gacca gaaca accaa tcagt tccta gctgt ctcaa
 481 aggga aactg ctcag ggccc actac aatca gaggt caatt ctcaa acatg tcgct gtccc
 541 tgtta gactt gtatt taggt cgagg ttaca atgtg tcatc tatag tcact atgac atccc
 601 aggga atgta tgggg gaact tacct agtgg aaaag cctaa tctga gcagc aaaag gtcag
 661 agttg tcaca actga gcatg taccg agtgt ttgaa gtagg tgtta tcaga aatcc gggtt
 721 tgggg gctcc ggtgt tccat atgac aaact atctt gagca accag tcagt aatga tctca
 781 gcaac tgtat ggtgg ctttg gggga gctca aactc gcagc ccttt gtcac gggga agatt
 841 ctatc acaat tccct atcag ggatc aggga aaggt gtcag cttcc agctc gtcaa gctag
 901 gtgtc tggaa atccc caacc gacat gcaat cctgg gtccc cttat caacg gatga tccag
 961 tgata gacag gcttt acctc tcatc tcaca gaggt gttat cgctg acaat caagc aaaat
1021 gggct gtccc gacaa cacga acaga tgaca agttg cgaat ggaga catgc ttcca acagg
1081 cgtgt aaggg taaaa tccaa gcact ctgcg agaat cccga gtggg cacca ttgaa ggata
1141 acagg attcc ttcat acggg gtctt gtctg ttgat ctgag tctga cagtt gagct taaaa
1201 tcaaa attgc ttcgg gattc gggcc attga tcaca cacgg ttcag ggatg gacct ataca
1261 aatcc aacca caaca atgtg tattg gctga ctatc ccgcc aatga agaac ctagc cttag
1321 gtgta atcaa cacat tggag tggat accga gattc aaggt tagtc cctac ctctt cactg
1381 tccca attaa ggaag caggc ggaga ctgcc atgcc ccaac atacc tacct gcgga ggtgg
1441 atggt gatgt caaac tcagt tccaa tctgg tgatt ctacc tggtc aagat ctcca atatg
1501 ttttg gcaac ctacg atact tccag ggttg aacat gctgt ggttt attac gttta cagcc
1561 caagc cgctc atttt cttac tttta tcctt ttagg ttgcc tataa agggg gtccc catcg
1621 aatta caagt ggaat gcttc acatg ggacc aaaaa ctctg gtgcc gtcac ttctg tgtgc
1681 ttgcg gactc agaat ctggt ggaca tatca ctcac tctgg gatgg tgggc atggg agtca
1741 gctgc acagt cаccc gggaa gatgg aacca atggg ggggg gggga gtggg ggggg gggga
1801 gtggg ggggg gggga gtcag gtgca gctgc ttcag ccagg ggcag aactt gtacg gcccg
1861 gcgca agcgt acgct tgtcc tgcaa aacga gtgga tatac gttta cctcc tactg gatca
1921 actgg gttaa acaga gaccg ggtca aggtc ttgag tggat cggta agatt ttccc cagtg
1981 attcc cacac taact ataat caaaa attta aggat aaagc tacgt tgacg gtcga taaat
2041 catct tccac cgcgt atatg caact gatat ctccg accag tgagg attct gccgt ttact
2101 attgc acaag agatt tcgac acgca gttct acgct atgga atact ggggt caggg gacтt
2161 ctgta acggt aagct ctggg ggggg gggga gtggg ggggg gggga gtggg ggggg gggga
2221 gtcaa attgt cctga cacaa agccc tacaa taatg agtgc atcac cggga caaaa ggtta
2281 caatt aactg ctctg cgatt agtag cgtga attac atgca ctggt atcag cagaa gcccg
2341 gttct tcacc taaac tttgg atata tgcta ctagt aagct gaccc tcgga gtacc ggctc
2401 gtttt agtgg aagtg gatca gggac cagtt acagc ttgac ggtta attca atggt tacag
  Q2 aagat gctac ttcct atttt tgcca ccagt ggtct tctta tcctc ctaca ttcgg ggctg
2521 gaact aaatt ggagt tgaag cgcag atag
```

Sequence Nomenclature	Coloring Schema	Sequence Numbering
Hemagglutinin Endodomain		1-102
Hemagglutinin Ectodomain		103-1772
GGGGS x3 Linker		1773-1817, 2178-2222
CD90 scFv VH sequence		1818-2177
CD90 scFv VL Sequence		2223-2539
Tail		2540-2549

Supplemental Figure 4: Variant H4 KO measles and targeting domain.

```
   1 atgaa cagag aacat cttat gattg ataga ccttа tgttt tgctg gctgt tctgt ttgtc
  61 atgtt tctga gcttg atcgg gttgc tagcc attgc aggca ttaga cttca tcggg cagcc
 121 atcta caccg cagag atcca taaaa gcctc agcac caatc tagat gtaac tactc aatcg
 181 agcat caggt caagg acgtg ctgac accac tcttc aaaat catcg gtgat gaagt gggcc
 241 tgagg acacc tcaga gattc actga cctag tgaaa ttcat ctctg acaag attaa attcc
 301 ttaat ccgga taggg agtac gactt cagag atctc acttg gtgta tcaac ccgcc agaga
 361 gaatc aaatt ggatt atgat caata ctgtg cagat gtggc tgctg aagag ctcat gaatg
 421 cattg gtgaa ctcaa ctcta ctgga gacca gaaca accaa tcagt tccta gctgt ctcaa
 481 aggga aactg ctcag ggccc actac aatca gaggt caatt ctcaa acatg tcgct gtccc
 541 tgtta gactt gtatt taggt cgagg ttaca atgtg tcatc tatag tcact atgac atccc
 601 aggga atgta tgggg gaact tacct agtgg aaaag cctaa tctga gcagc aaaag gtcag
 661 agttg tcaca actga gcatg taccg agtgt ttgaa gtagg tgtta tcaga aatcc gggtt
 721 tgggg gctcc ggtgt tccat atgac aaact atctt gagca accag tcagt aatga tctca
 781 gcaac tgtat ggtgg ctttg gggga gctca aactc gcagc ccttt gtcac gggga agatt
 841 ctatc acaat tccct atcag ggatc aggga aaggt gtcag cttcc agctc gtcaa gctag
 901 gtgtc tggaa atccc caacc gacat gcaat cctgg gtccc cttat caacg gatga tccag
 961 tgata gacag gcttt acctc tcatc tcaca gaggt gttat cgctg acaat caagc aaaat
1021 gggct gtccc gacaa cacga acaga tgaca agttg cgaat ggaga catgc ttcca acagg
1081 cgtgt aaggg taaaa tccaa gcact ctgcg agaat cccga gtggg cacca ttgaa ggata
1141 acagg attcc ttcat acggg gtctt gtctg ttgat ctgag tctga cagtt gagct taaaa
1201 tcaaa attgc ttcgg gattc gggcc attga tcaca cacgg ttcag ggatg gacct ataca
1261 aatcc aacca caaca atgtg tattg gctga ctatc ccgcc aatga agaac ctagc cttag
1321 gtgta atcaa cacat tggag tggat accga gattc aaggt tagtc ccgca ctctt cactg
1381 tccca attaa ggaag caggc ggaga ctgcc atgcc ccaac atacc tacct gcgga ggtgg
1441 atggt gatgt caaac tcagt tccaa tctgg tgatt ctacc tggtc aagat ctcca atatg
1501 ttttg gcaac ctacg atact tccgc agttg aacat gctgt ggttt attac gttta cagcc
1561 caagc cttga gcttt cttac tttta tcctt ttagg ttgcc tataa agggg gtccc catcg
1621 aatta caagt ggaat gcttc acatg ggacc aaaaa ctctg gtgcc gtcac ttctg tgtgc
1681 ttgcg gactc agaat ctggt ggaca tatca ctcac tctgg gatgg tgggc atggg agtca
1741 gctgc acagt cacccc gggaa gatgg aacca atggg ggggg gggga gtggg ggggg ggggа
1801 gtggg ggggg gggga gtcag gtgca gctgc ttcag ccagg ggcag aactt gtacg gcccg
1861 gcgca agcgt acgct tgtcc tgcaa aacga gtgga tatac gttta cctcc tactg gatca
1921 actgg gttaa acaga gaccg ggtca aggtc ttgag tggat cggta agatt ttccc cagtg
1981 attcc cacac taact ataat caaaa attta aggat aaagc tacgt tgacg gtcga taaat
2041 catct tccac cgcgt atatg caact gatat ctccg accag tgagg attct gccgt ttact
2101 attgc acaag agatt tcgac acgca gttct acgct atgga atact ggggt caggg gacтt
2161 ctgta acggt aagct ctggg ggggg gggga gtggg ggggg gggga gtggg ggggg ggggа
2221 gtcaa attgt cctga cacaa agccc tacaa taatg agtgc atcac cggga caaaa ggtta
2281 caatt aactg ctctg cgatt agtag cgtga attac atgca ctggt atcag cagaa gcccg
2341 gttct tcacc taaac tttgg atata tgcta ctagt aagct gaccc tcgga gtacc ggctc
2401 gtttt agtgg aagtg gatca gggac cagtt acagc ttgac ggtta attca atggt tacag
2461 aagat gctac ttcct atttt tgcca ccagt ggtct tctta tcctc ctaca ttcgg ggctg
2521 gaact aaatt ggagt tgaag cgcag atag
```

Sequence Nomenclature	Coloring Schema	Sequence Numbering
Hemagglutinin Endodomain		1-102
Hemagglutinin Ectodomain		103-1772
GGGGS x3 Linker		1773-1817, 2178-2222
CD90 scFv VH sequence		1818-2177
CD90 scFv VL Sequence		2223-2539
Tail		2540-2549
Hemagglutinin Mutations		1368-1370, 1524-1526, 1566-1571

Supplemental Figure 5: Measles H Plasmid Map.

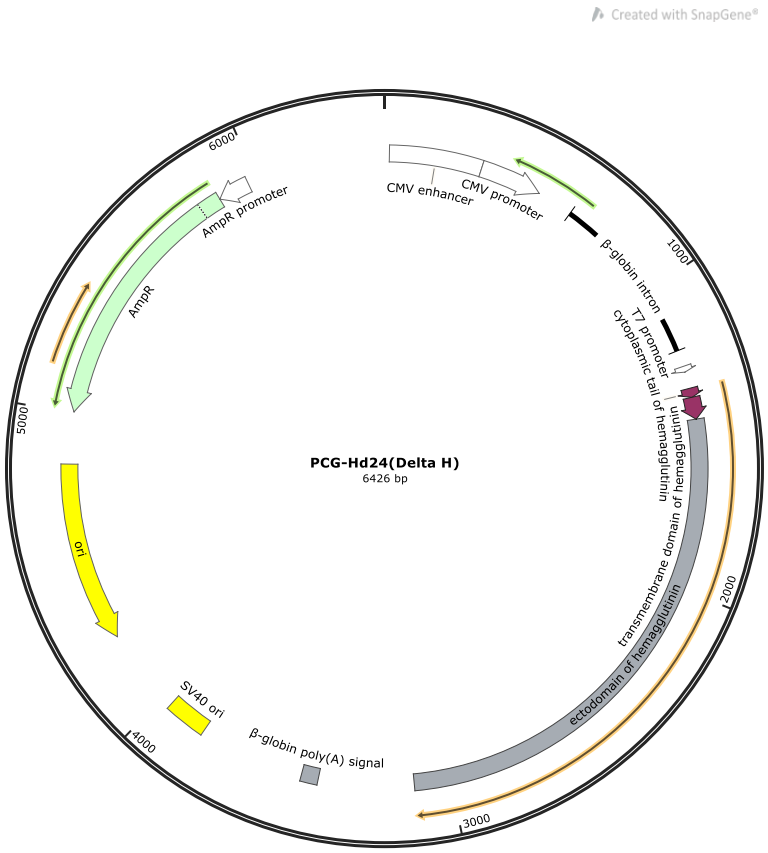

Supplemental Figure 6: Measles H CD90 scFv Plasmid Map

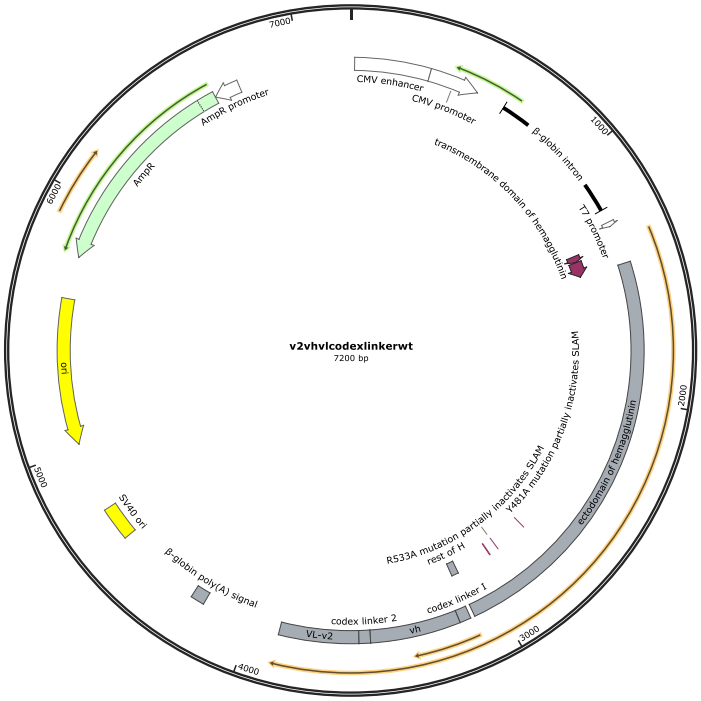

Supplemental Figure 7: Measles F Plasmid Map.

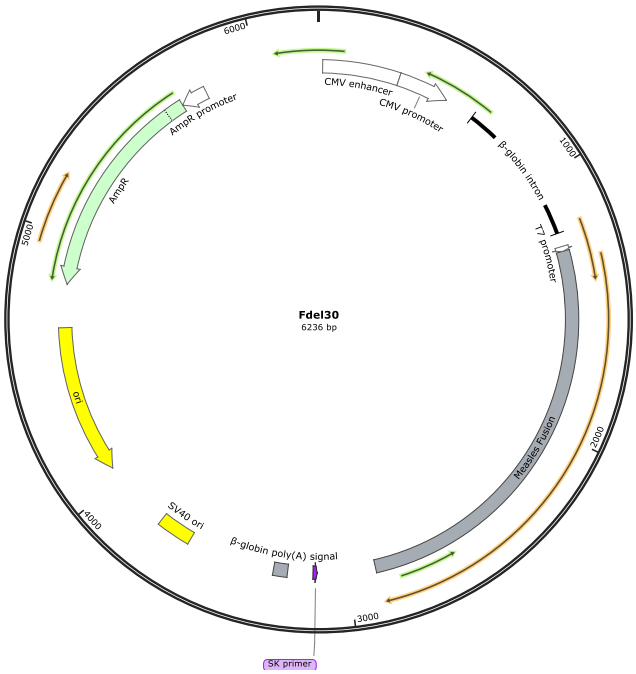

Chapter 2: Co-LOCKR Targeting:

Introduction:

Hematopoietic stem cell (HSC) gene therapy is a promising treatment option for a variety of genetic diseases affecting the hematopoietic system. However, currently available approaches are performed *ex vivo* and require a highly sophisticated infrastructure like bone marrow transplantation. In addition, current approaches target $CD34^+$ hematopoietic stem and progenitor cells (HSPCs) containing less than 1% true HSCs[23, 25]. Thus, *ex vivo* HSC gene therapy is inefficient, expensive, and carries the risk for off-target effects in non-HSCs. To overcome these limitations, we propose to develop a highly specific, portable, and safe HSC-targeted gene therapy approach that will allow *in vivo* HSC gene therapy.

Previous work in the Kiem Lab has shown that the $CD90^+$ subset of $CD34^+$ HSPCs is highly enriched for HSCs and exclusively responsible for rapid recovery as well as robust long-term multilineage engraftment[34]. Directly targeting this marker is a logical method to edit the key cells for effective gene therapy. However as previously mentioned other cells such as mesenchymal stem cells and neurons express CD90 on their surface. Other markers for HSCs such as CD133, CD34, or CD117 are both present more impure populations of HSC's as well as in other cell types across the body. One way we have explored to avoid this potential off target effects is to use the CO-LOCKR system developed by the Baker lab.

To achieve target specificity and avoid off-targets, the Baker Lab has recently designed colocalization-dependent protein switches (Co-LOCKR) able to specifically target tumors and avoid off-target delivery to healthy tissues using Bcl2-targeted CAR T cells [40, 41]. We have worked together to design variants of their targeting moieties combined with our lentiviral systems to target their highly modifiable Co-LOCKR protein complex. We have begun work to utilize these systems in vivo In the future, further developments of this technology could enable HSC-specific providing the foundation for safe and efficient *in vivo* HSC gene therapy applications that would be portable with a simple local injection and cost effective needing minimal infrastructure. In addition, the flexibility of the cargo within the lentiviral system would enable easy modifications to treat a variety of genetic and infectious diseases with this efficacious form of *in vivo* gene therapy.

Results:

Design, production, and hydrodynamic titration of BCL-2 Targeted Measles and VSVG Viruses

We and others have previously shown that the hemagglutinin protein of measles is highly receptive to modifications both in its own targeting of CD46 and CD150 as well as to additions of scFvs and other targeting moieties on its surface[74]. The Baker lab had previously shown that taking advantage of the BCL-2 BIM protein combination, an intracellular interaction, was feasible to allow CAR-T cells displaying BCL-2 on the surface to target a BIM protein engineered as the sequestered recruitment peptide in the CO-LOCKR complex. We here were able to clone the BCL-2 complex on the end of a linker similar to what was used in the CD90 scFv work on the extracellular portion of the measles hemagglutinin on the surface of a pseudotyped lentivirus

(Supplementary Figure 1) (Figure 1). In addition, we developed a new virus paradigm here, building off of work that used a modified vesicular stomatitis virus g protein (VSVG) knocked out for its native low-density-lipoportein(LDL) targeting with a CD8 linker/leader and hinge portion to BCL-2, so as to have additional options for future experiments(Supplementary Figure 2-3)[75].

The inability to reliably titrate these viruses necessitated a novel form to establish our virus's ability to transduce, and we again turned to the Zetaviewer platform. Successful loading of viral capsules and loading efficiency was determined staining the particles with SYBR II. The number of mRNA-loaded viral particles was variable across batches. However, the loading efficiency of viral particles (frequency of mRNA-loaded particles within total particles) was very consistent averaging at 10 to 20 % with no obvious differences due to the modification made. The VSVG version of our virus consistently performed 5 to 10x higher concentration of loaded particles when compared to the measles pseudotyped version of our viruses(Figure 2).

Next, we measured the size of our vector variants in the presence and absence of the HER2BIM-mCherry protein to test for the viruses targeting abilities(**Figure 3B**). The vector alone was in the range 110-130nm. The protein alone was measured at 160nm, and when incubated with the targeted virus a and measured with the 520nm laser filter to only account for things bound to the MCherry flourescent protein a new peak was observed shifted to 280nm, indicating interaction and a subsequent size increase(Figure 3)

We initially utilized a Her2-BIM fusion protein as a positive control to test our virus's basic transduction abilities and were able to see strong specific targeting (Figure 4) several fold over background noise. When using Co-LOCKR proteins we observed low but specific viral targeting

using the Co-LOCKR proteins to K562 cells displaying the targeting markers many times greater than background signal. No targeting was observed in cells lacking the targeting surface molecules or in the absence of any of the Co-LOCKR components (Figure 5).

CO-LOCKR protein improvements and enhancements

While initial results were encouraging, the lower targeting in the Co-LOCKR compared to the Her2-BIM positive control led us to believe further improvements could be made to the Co-LOCKR proteins to improve their ability to lead the virus. A key issue we identified was that the Co-LOCKR protein complex was larger than the Her2-BIM fusion protein, causing the virus to be further away and lessening the chance that it could engage in fusion with the cellular membrane. We attempted to ameliorate this problem by shortening the linker between the targeting ligand and the Co-LOCKR cage, as well as to flip the orientation of the linker in relation to the rest of the cage protein, necessitating the virus be closer to the cell when it interacts with its targeting ligand. Testing with these improved variants of the Co-LOCKR complex showed improved targeting efficacy while not negatively affecting specificity of targeting (Figure 6).

In Vivo Tumor Targeting Model:

Next, we moved to evaluating the targeting capabilities of these protein virus combinations in the bone marrow compartment of mice. We chose to use Raji cells as our cell line and began by determining the growth kinetics of the cells within the bone marrow of NSG and NBSGW mice. We went through a series of experiments determining the ideal conditions for cancer growth and what would be the ideal time to inject the virus and Co-LOCKR components. We discovered that the Raji's cells would not traffic through the body to the bone marrow with our without total body irradiation(TBI). We increased our dosage of Raji cells and moved to intra

femoral injections of the cancer cells and found this to be more successful. We eventually settled on NSG mice being injected with 2 million Raji cells, with TBI prior to cancer cell injection, and allowed for 4-5 days of cancer growth to ensure ideal numbers of target cells as our ideal conditioning regimen (Figure 7).

After establishing the protocol, we began experiments directly injecting the BCL-2 KO measles and VSVG versions of our virus with mScarlet reporter gene and Co-LOCKR components into the bone marrow of mice that contained both EGFR+HER2+and EGFR-HER2- Raji cells that had been allowed to grow for 5 days. GFP positive Raji cells were easily distinguishable from mouse cells(Figure 8).Additionally, the ratio between the double positive and negative cells contained in the bone marrow was close to close to 1/1 in all conditions, ensuring adequate amounts of off target cells to confirm the validity of the targeting(Figure 9). 3 days after the protein and virus injection we harvested the mouse bone marrow we observed low but extremely specific targeting of the on-target cells and no off-target effects via flow cytometry (Figure 10). This was an encouraging finding, and we next proceeded to injection of the virus and Co-LOCKR components via tail vein injection, hypothesizing that this would be more difficult for the virus and proteins to travel the entirety of the circulatory system and enter the bone marrow prior to finding and transducing cells successfully. Excitingly, we did observe specific on-target transduction and no off-target effects, suggesting the viruses as well as Co-LOCKR proteins and Bcl2-targeted viral vectors are stable, resist serum inactivation, and can travel the full length of a murine circulatory system, enter the bone marrow, and successfully transduce cells even in hardly accessible tissues(Figure 10).

While this work is exciting in its implications, we are continuing to expand the possibilities of this system. Modified surface markers that are overexpressed are a useful diagnostic but not expressive of real conditions. Therefore, the next step we are pursuing is using CD3/CD28 targeted Co-LOCKR proteins with the long-term goal of using this to create CAR T-cells in vivo. Early data suggests that this system is viable, although more optimizations will be necessary.

Discussion:

Here we have shown that Co-LOCKR proteins combined with BCL2-engineered lentiviral vectors can localize target cells ex vivo as well as in vivo with a remarkably high on-target specificity. This system was incorporated into our previous hydrodynamic titering system, enabling easy quality control of the viruses. Modifications to the Co-LOCKR proteins resolved the issues of distance from virus to cell and the problems that created with regards to viral entry. Targeted viruses as well as Co-LOCKR proteins and Bcl2-targeted viral vectors are stable, resist serum inactivation, and can travel the full length of a murine circulatory system, enter the bone marrow, and successfully transduce cells even in hardly accessible tissues. Most importantly, Cage and Key targeting molecules are easily exchanged for the targeting of hematopoietic stem cells (HSCs) such as CD90 and CD34 or T cells. The ability to target bone marrow-resident cells highly specifically via an intravenous administration of this novel delivery system provides a new strategy to perform HSC gene therapy in vivo without the need of mobilization.

Current Methods of targeting for *in vivo* gene therapy applications still have major hurdles to overcome. The common use of one cell surface marker as their targeting moiety can cause off target effects if unwanted cell types display the marker of interest. In the case of

HSC's, some of the common surface markers such as CD117, CD34, and CD133 are present on other cell types throughout the body, meaning *in vivo* applications have off target potentials. This possibility complicates the viability *in vivo* gene therapies.

While this study makes important improvements towards the viability of *in vivo* gene therapy applications, more study is necessary. This study primarily focused on the specific off target effects that could be present on the "off target" cancer cell population. More extensive testing will need to be performed on how the viruses potentially interact with cells within the body and whether off target events occur. Currently we have plans to use luciferase loaded versions of our viruses to evaluate this in a systemic manner in our mouse models. Additionally, the current in vivo gene editing we observe is very low. This can be ascribed to a variety of factors, from middling virus concentration to various anti-viral actions taking place within the bloodstream. Devising methods to increase this transduction rate are also ongoing.

The success of this systems utilizing cancer cell markers for virus targeting, and our preliminary data with T cell markers, suggest this system could be an effective way to enhance all types of gene therapies. In particular, the ability for the proteins and viruses to enter the bone marrow and still specifically transduce cells, might remove the need for stem cell mobilization for *in vivo* gene therapies, an improvement that would reduce the negative effects of the treatment. This technique can be used to further optimize *ex vivo* transduction pipelines, as well as answering key targeting questions to make *in vivo* gene therapies a viable option for patients. While the testing in this study focused on lentiviruses, the technology is applicable to other delivery vehicles, such as nanoparticles and further virus types not explored here. In

summary this study moves the field of gene therapy slightly closer to a new paradigm of *in vivo* applications.

Chapter 2 Figures:

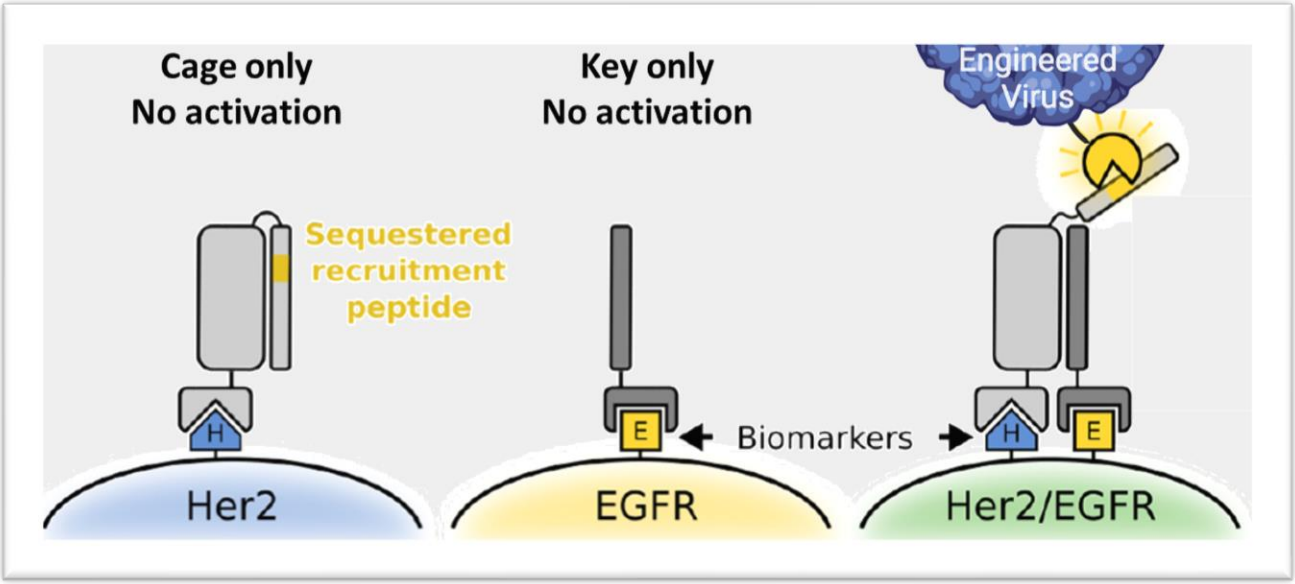

Figure 1: Schematic depicting Co-LOCKR virus targeting plan:

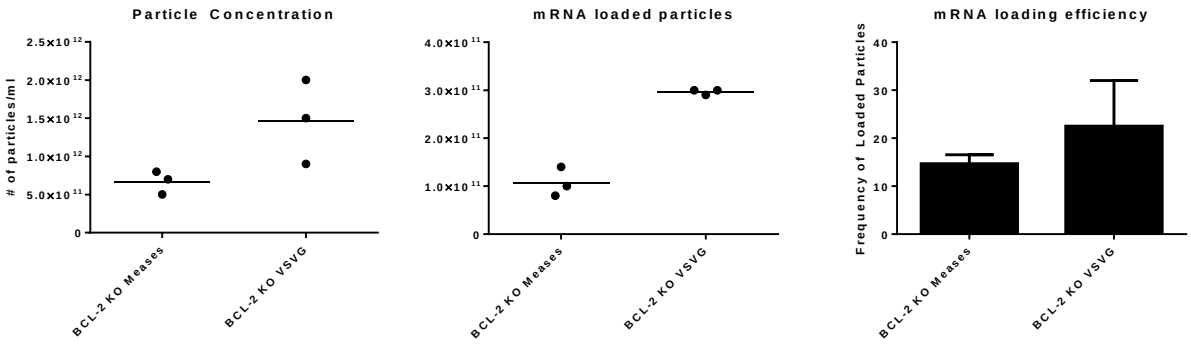

Figure 2 Hydrodynamic Titer BCL-2 Targeted Viruses: Top figure, schematic describing BIM-BCL-2 targeted virus interaction. From left concentration of viral particles per ml culture medium

harvested. Middle is concentration of RNA-loaded viral particles per ml culture medium measured with SYBR II. And right graph is RNA loading efficiency calculated based on values from the previous two graphs.

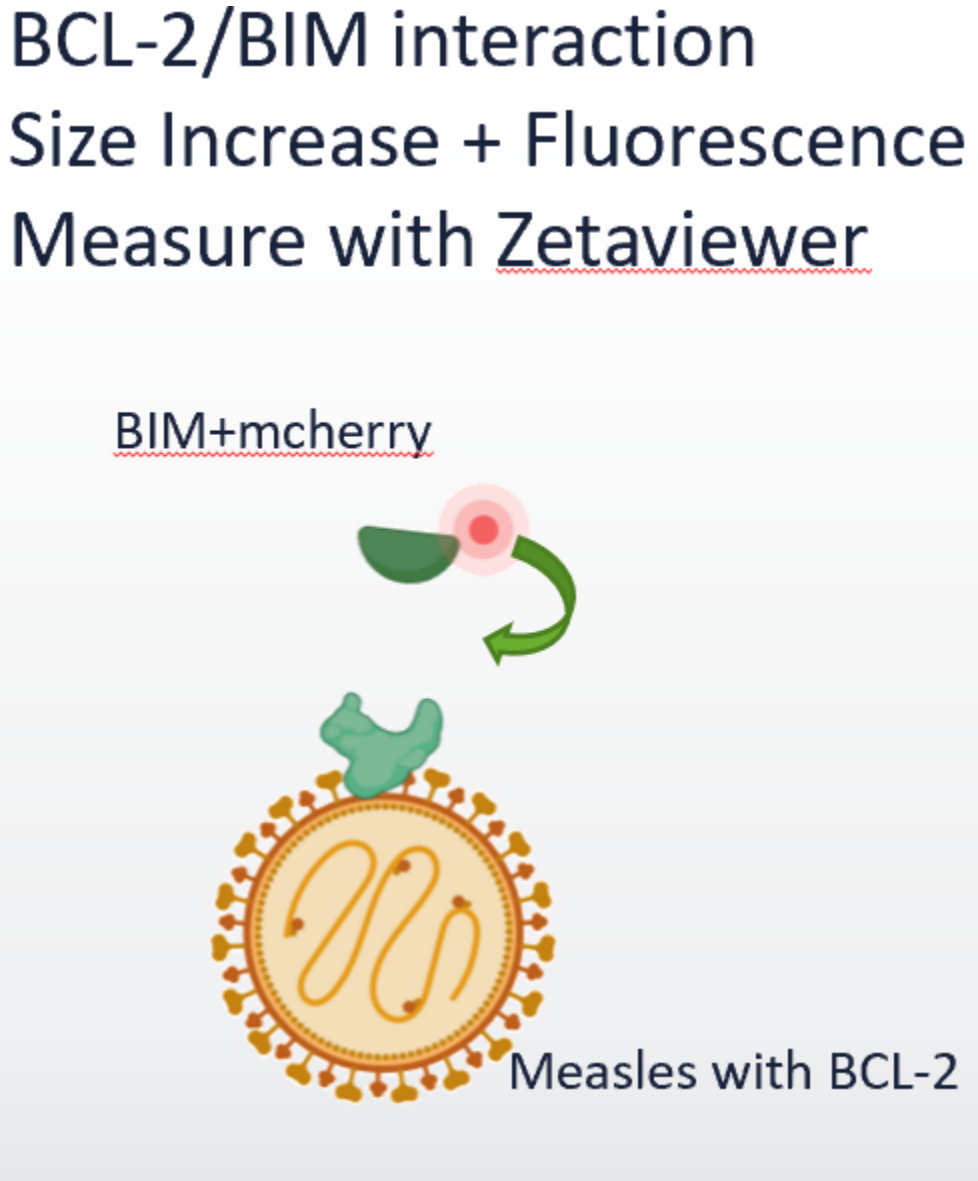

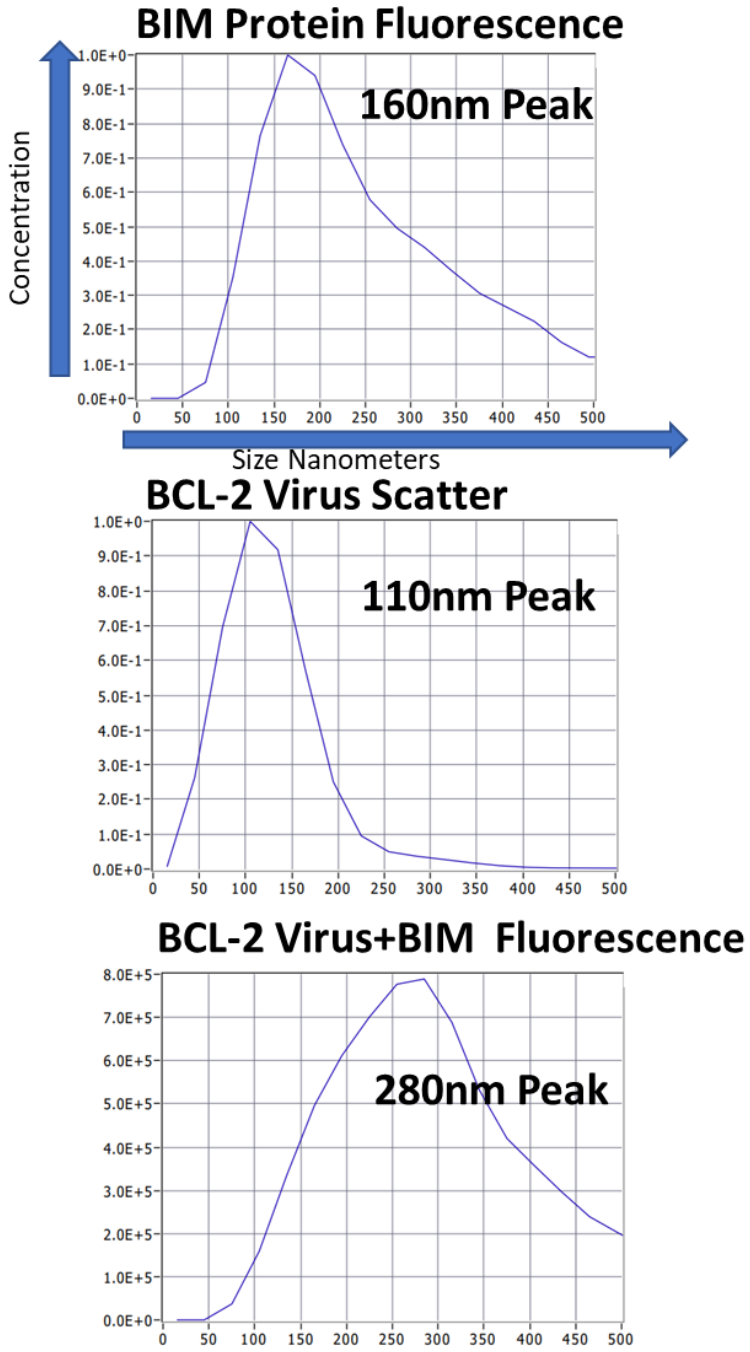

Figure 3 BCL-2 KO Virus Hydrodynamic Interaction: Hydrodynamic size correlation to confirm BCL-2 BIM interaction. Size of BIM-mCherry fusion protein (top row). Size of BCL-2 targeted virus (middle row). Size of BCL-2 Virus incubated with BIM-MCherry fusion protein for 30 minutes (bottom row). Numbers indicate size of observed peak in nanometers.

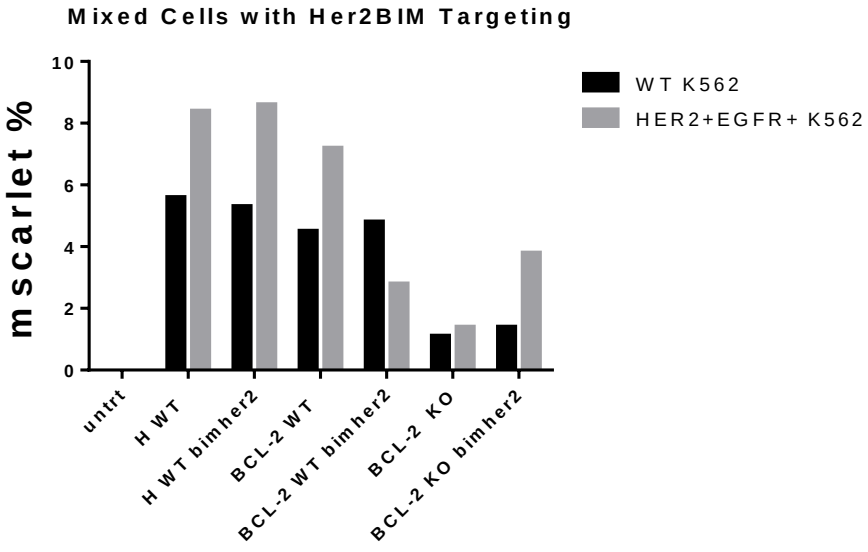

Figure 4 HER2BIM Targeting: plot of data showing both untargeted(H) BCL-2 targeted (BCL-2) and BCL-2 targeted with native targeting knocked out (BCL-2 KO) virus against both EGFR-HER2- K562 and HER2+ EGFR+ K562 cells both in the presence and absence of the bim-anti-her2 binding protein. Bim-anti-her2 protein should catalyze bcl-2 targeted viral fusion when the anti-her2 portion binds to HER2 on the surface of cells. Her2 positive K562 cells show significant increase in transduction with the BCL-2 and BCL-2 KO virus in the presence of bim-anti-her2.

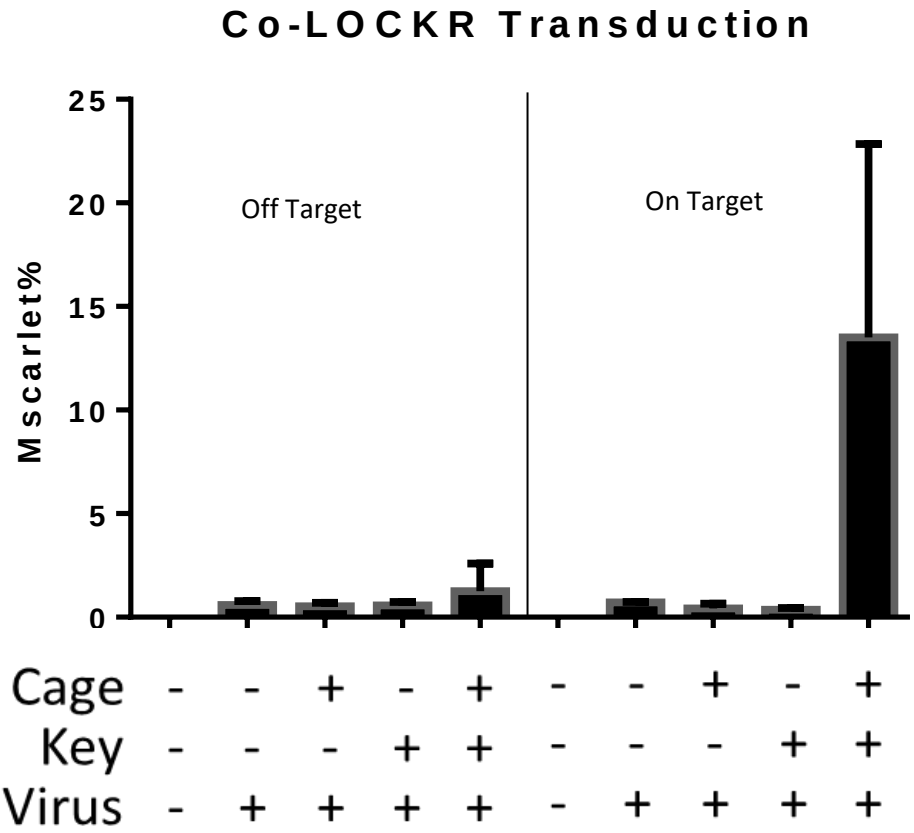

Figure 5 In Vitro Co-LOCKR: BCL-2 KO VSVG Virus was evaluated on Raji EGFR+HER2+(on target) or Raji EGFR-HER2-(off target) cell lines in the presence or absence of Co-LOCKR components. Off target cell lines still display lesser amounts of target surface antigen, causing some leakage.

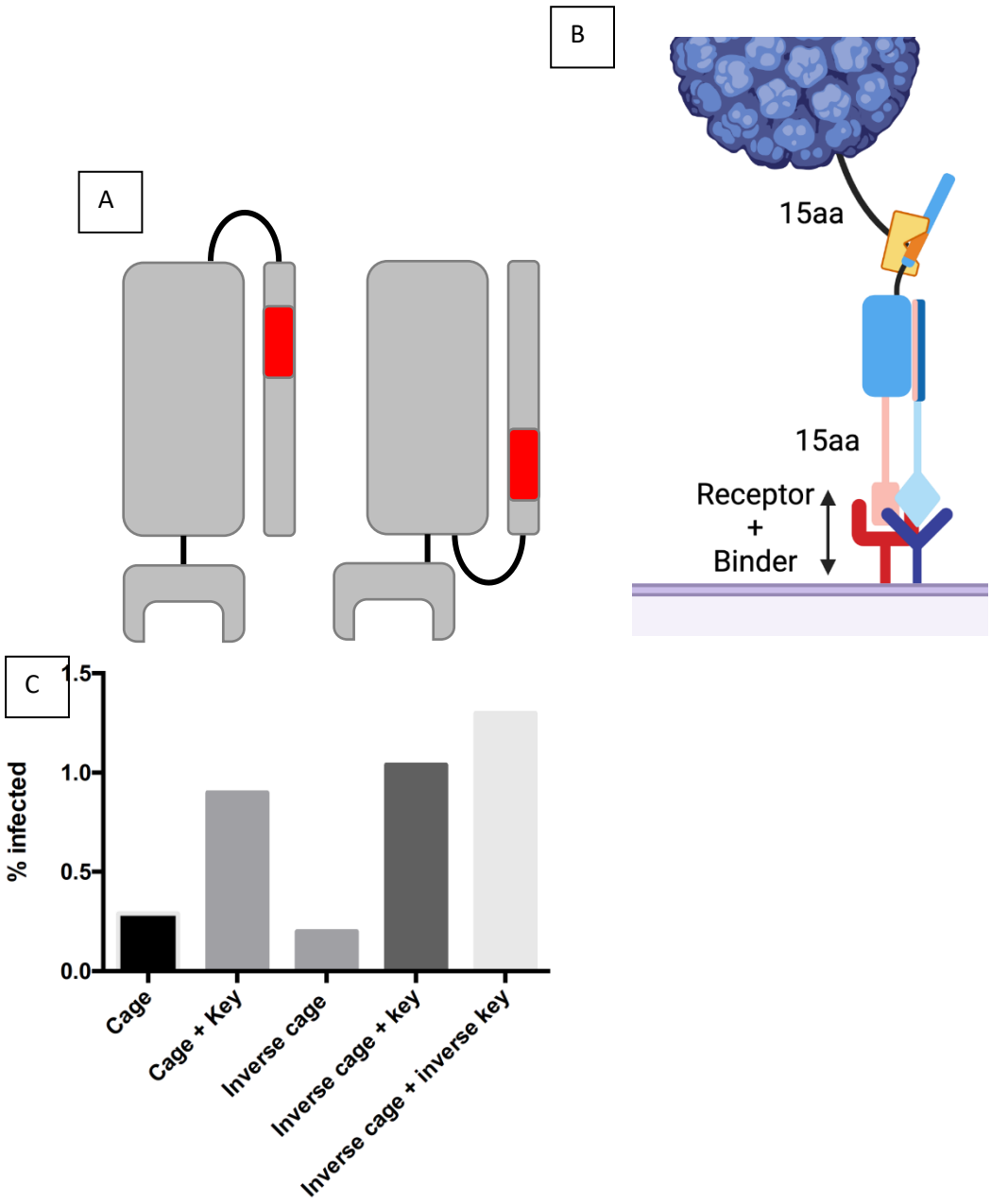

Figure 6 Co-LOCKR Protein Modifications: Figure depicting goal of Co-LOCKR modification as well as figure showing distance problem for viral fusion(A-B). K562 EGFR+HER2+ cells were transduced with VSVG KO BCL-2 targeted virus and incubated with indicated modified cage and/or key combination. Plot showing observed transduction for new protein variant's ability when transduced with BCL-2 KO VSVG virus(C). Inverting cage and key to bring virus closer to cell shows increased efficacy without increasing off target effects.

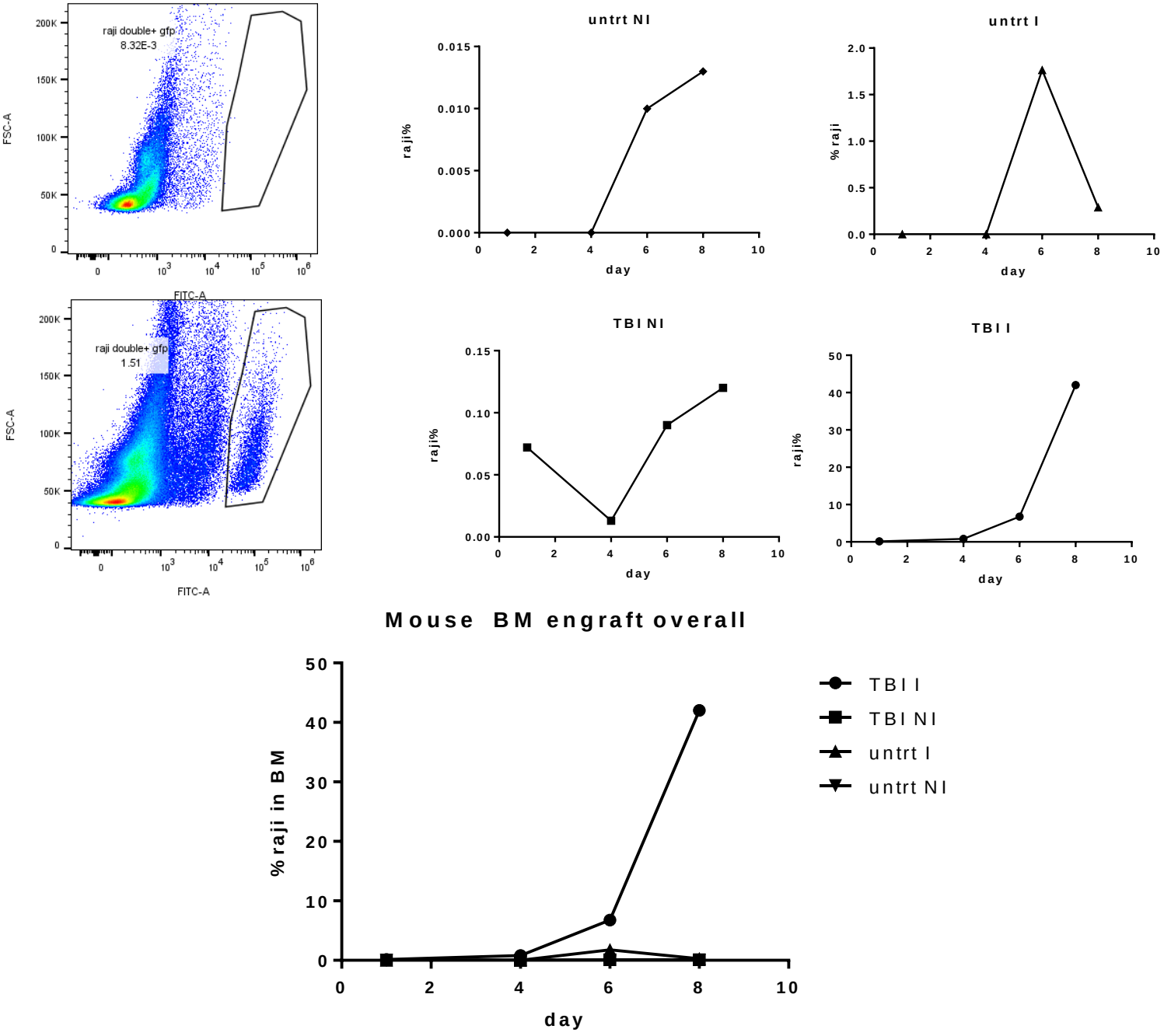

Figure 7 Raji Engraftment Bone Marrow: Engraftment kinetics of Raji GFP+ cells into NSG Mouse Femoral Bone Marrow. Raji's were gated from mouse cells using GFP as the marker and were examined over 8 days in both TBI and non-TBI conditions, as well as investigating the injected(I) and non-injected (NI) femoral bones to see if there was migration between bones of the Raji cells.

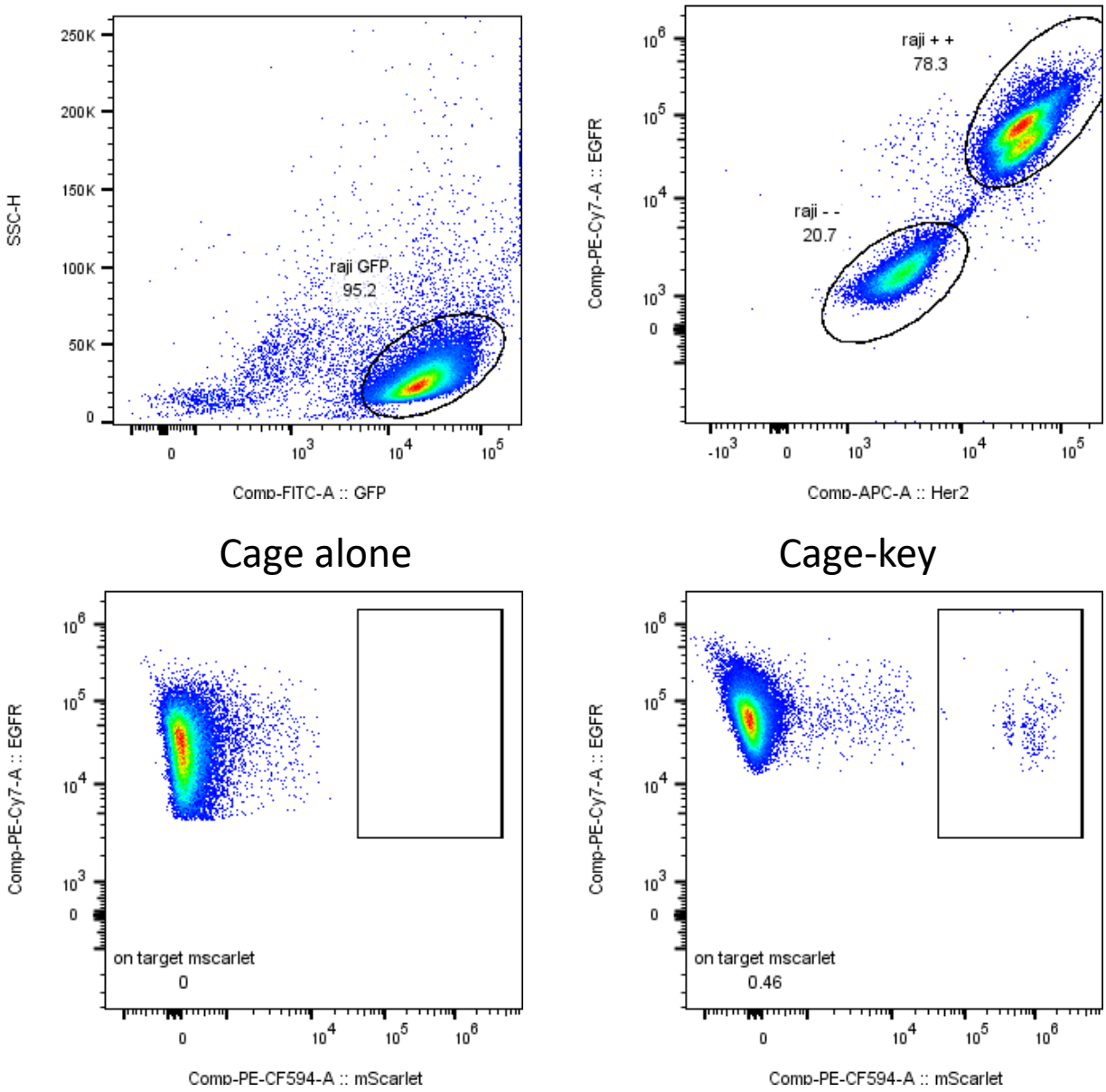

Figure 8 In Vivo Flow cytometry analysis: Example flow plots for mouse in vivo virus and Co-LOCKR experiments. Top left shows side scatter vs GFP, the Raji cells showing up distinctly as GFP+. Top Right shows EGFR vs HER2, showing the distinction vs the Double positive vs double negative populations for targeting. Bottom two graphs show the mScarlet positivity in the cage vs cage key populations with stringent gating as an example.

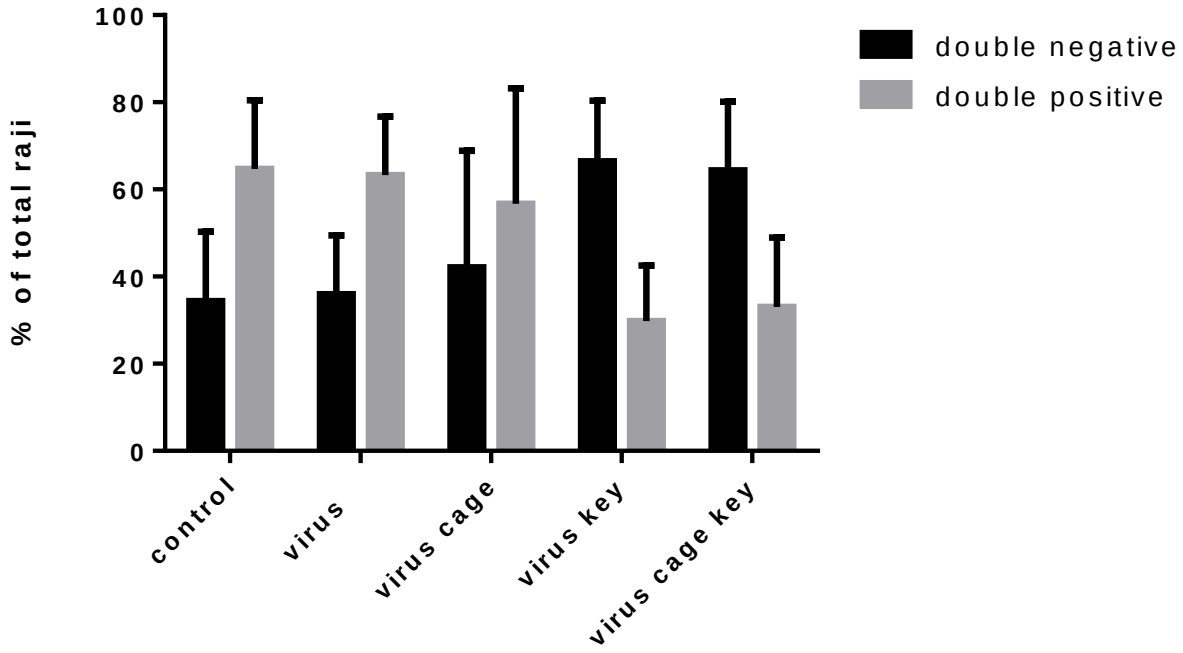

Figure 9 Raji Double Positive to Negative Ratios: Plot showing the cellular ratio of EGFR+HER2+(double positive) vs EGFR-HER2-(double negative) Raji cells in the bone marrow across of mouse *in vivo* all experiments performed during the final analysis. Cells averaged close to a 1-1 ratio of on to off target cells. Future experiments will contain more dilute concentrations of on-target cells.

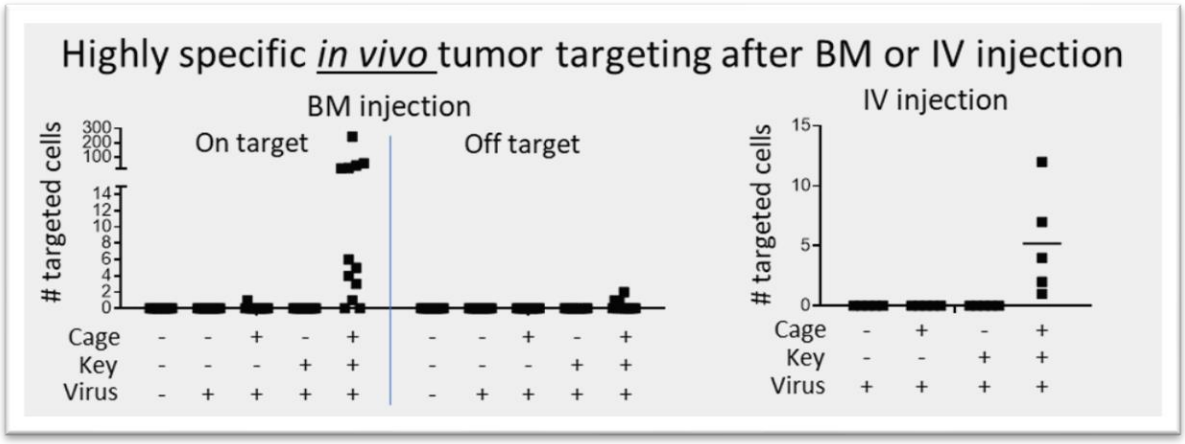

Figure 10 In vivo Co-LOCKR: Results from *in vivo* experiments in mice with direct bone marrow(BM) administration of BCL-2 KO virus (both measles and VSVG) and intravenous(IV) tail vein administration. Bone marrow compartment was collected from mice, allowed to sit in culture for 3 days, then collected via flow cytometry. No off-target effects were observed in mouse cells. On target is EGFR+ HER2+ Raji cells and off target is EGFR-HER2- Raji cells. Only on target cells were used in this first round of experiments in IV injection. Future experiments will contain off target cells as well.

Supplementary Figure 1 BCL-2 Measles KO Sequence:

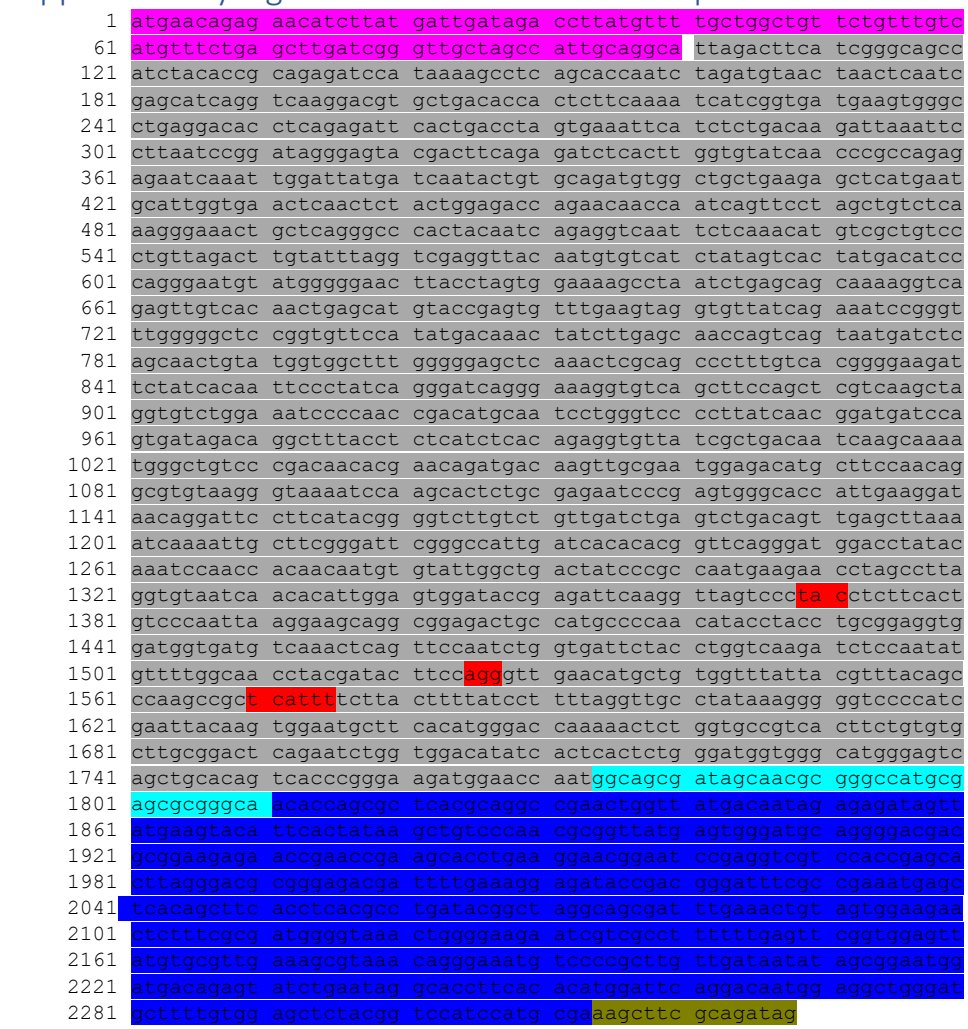

Sequence Nomenclature	Coloring Schema	Sequence Numbering

Hemagglutinin Ectodomain		1-102
Hemagglutinin Endodomain		103-1772
Linker		1773-1817
BCL-2 Sequence		1811-2313
Tail		2314-2328
Hemagglutinin KO Mutations		1368-1370, 1524-1526, 1566-1571

Supplementary Figure 2: VSVG KO plasmid

```
   1 atgaagtgcc ttttgtactt agccttttta ttcattgggg tgaattgcaa gttcaccata
  61 gtttttccac acaaccaaaa aggaaactgg aaaaatgttc cttctaatta ccattattgc
 121 ccgtcaagct cagatttaaa ttggcataat gacttaatag gcacagcctt acaagtcaaa
 181 atgccc   a gtcacaaggc tattcaagca gacggttgga tgtgtcatgc ttccaaatgg
 241 gtcactactt gtgatttccg ctggtatgga ccgaagtata taacacattc catccgatcc
 301 ttcactccat ctgtagaaca atgcaaggaa agcattgaac aaacgaaaca aggaacttgg
 361 ctgaatccag gcttccctcc tcaaagttgt ggatatgcaa ctgtgacgga tgccgaagca
 421 gtgattgtcc aggtgactcc tcaccatgtg ctggttgatg aatacacagg agaatgggtt
 481 gattcacagt tcatcaacgg aaaatgcagc aattacatat gccccactgt ccataactct
 541 acaacctggc attctgacta taaggtcaaa gggctatgtg attctaacct catttccatg
 601 gacatcacct tcttctcaga ggacggagag ctatcatccc tgggaaagga gggcacaggg
 661 ttcagaagta actactttgc ttatgaaact ggaggcaagg cctgcaaaat gcaatactgc
 721 aagcattggg gagtcagact cccatcaggt gtctggttcg agatggctga taaggatctc
 781 tttgctgcag ccagattccc tgaatgccca gaagggtcaa gtatctctgc tccatctcag
 841 acctcagtgg atgtaagtct aattcaggac gttgagagga tcttggatta ttccctctgc
 901 caagaaacct ggagcaaaat cagagcgggt cttccaatct ctccagtgga tctcagctat
 961 cttgctccta aaaacccagg aaccggtcct gctttcacca taatcaatgg taccctaaaa
1021 tactttgaga ccagatacat cagagtcgat attgctgctc caatcctctc aagaatggtc
1081 ggaatgatca gtggaactac cacagaagcc gaactgtggg atgactgggc accatatgaa
1141 gacgtggaaa ttggacccaa tggagttctg aggaccagtt caggatataa gtttccttta
1201 tacatgattg gacatggtat gttggactcc gatcttcatc ttagctcaaa ggctcaggtg
1261 ttcgaacatc ctcacattca agacgctgct tcgcaacttc ctgatgatga gagtttattt
1321 tttggtgata ctgggctatc caaaaatcca atcgagcttg tagaaggttg gttcagtagt
1381 tggaaaagct ctattgcctc ttttttcttt atcatagggt taatcattgg actattcttg
1441 gttctccgag ttggtatcca tctttgcatt aaattaaagc acaccaagaa aagacagatt
```

Sequence Nomenclature	Coloring Schema	Sequence Numbering
VSVG Knockout Mutations		187-189, 1108-1110

Supplementary Figure 3: BCL-2 Hinge/Linker Plasmid

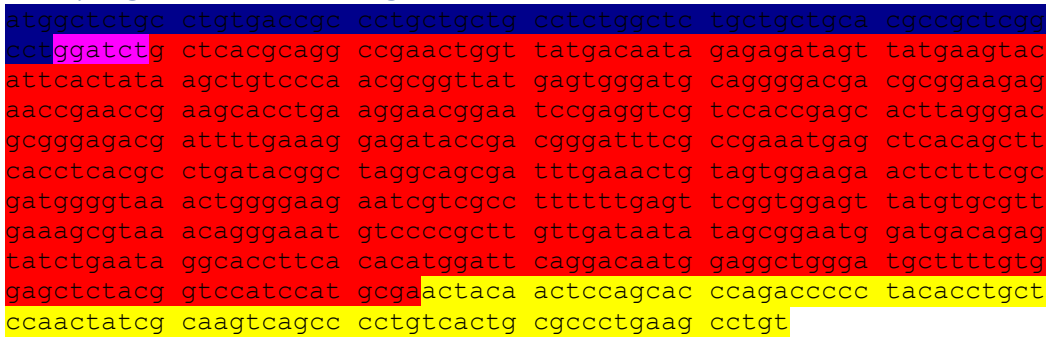

Sequence Nomenclature	Coloring Schema	Sequence Numbering
CD8 Leader		1-63
GS Linker		64-69
BCL-2		70-564
CD8 Hinge		565-645

Overall Conclusions:

In vivo gene therapies represent a way to take the most advanced knowledge and techniques for curing a variety of genetic diseases and democratize its access to patients in resource impoverished areas. Genetic disorders such as sickle cell disease have viable therapeutic options available, but *ex vivo* gene therapy remains the gold standard of treatment. *Ex vivo* modification needs extensive medical infrastructure and trained staff, which reduces its availability in substantial areas of the world. A single shot of an *in vivo* based gene therapy would reduce the need for infrastructure and increase potential access. One substantial hurdle to be solved for *in vivo* therapies to work is to develop effective ways to target gene therapy vehicles to cells of interest.

Here we have developed two platforms which can be utilized to enhance gene therapies through their targeting capabilities. We have taken a marker associated with a refined HSC population developed a novel targeting moiety against it and incorporated this targeting capability into an established virus system and shown its ability to successfully transduce HSC's.

In addition, we have worked with collaborators to show that the Co-LOCKR system can be used for specific and combinatorial viral targeting, and that this functions in vivo, and is not limited to artificially increased cancer markers. While work remains, these accomplishments represent important steps forward in solving the problem of targeting for *in vivo* gene therapies.

These improvements represent small steps towards developing flexible platforms with which *in vivo* therapies can be continued to be evaluated in preclinical and hopefully one day clinical models. While the gene transfers that were used were fluorescent markers, these could be easily swapped for therapeutically relevant genes within the well-established lentiviral system. Viruses however have limits, particularly in their ability to transiently deliver gene editing reagents. In this respect, nanoparticles loaded with mRNA can excel, and this thesis is actively being pursued to target nanoparticles for transient delivery of Cas9 reagents that will further explore its therapeutic possibilities. Additionally, all the improvements discussed above can be quickly folded into existing *ex vivo* gene therapy techniques, improving their targeting ability, reducing off-target effects, and reducing the amounts of reagents that would be needed due to the increased efficacy of targeting the cell types of interest.

Future Directions:

This work will hopefully represent a stepping off point for future in vivo directed therapies. There are a few more specific avenues of study that would be necessary for this platform to continue through preclinical development though. These include further investigating potential off target effects, more broadly characterizing the nature of the targeting mechanistically, addressing potential immune responses, observing how gene

expression of relevant therapeutic genes occurs, moving into larger animal models such as non-human primates, and broad manufacturing challenges. In addition, investigating how these targeting systems work in vehicles other than lentiviruses will be worth investigating.

Regarding off target effects, these can be modeled *in vitro* via the usage of ever more dilute populations of the cells of interest within mixtures of either white blood cells, whole blood, or other combinations. Increasing the dilution and dosage of virus can address how the targeting will be affected and investigate how various immune cells and natural antibodies will react to the various viruses described here. In animal models, replacing the mScarlet transfer gene we have utilized with a luciferase gene will enable rapid diagnostics of virus biodistribution to detect off target events[76]. This in addition to finer analysis of the various mouse organ systems with qPCR and additional flow cytometry will round out the investigation into off target events.

Investigating the nature of how the targeting works mechanistically is also of great interest. Viruses using CD90 as an entry pathway via micropinocytosis is already known, and some methods have been established to investigate that, including blocking certain endocytosis pathways with inhibitors to see if these lentivirus constructs utilize similar pathways. Co-LOCKR components are thus far unknown if they trigger the virus's natural fusion pathway or enter via another system, but similarly to before, inhibitors could answer some of these questions, as well as making modifications to the viruses own fusion proteins and seeing if that inhibits its ability to enter. We are currently working on establishing the structure of Thy-1 and its binding to antibodies and scFv's through electron microscopy, as well as running microscopy experiments to track how endocytosis occurs via CD90 targeting. Using this knowledge of our

CD90 scFv's binding locations, we are working to mutate those binding locations on CD90 and mutate them to ablate binding while not otherwise negatively effecting cellular function. With this modified CD90, we will then be able to use our targeting platform to target and eliminate non-modified HSC's while the HSC's with modified CD90 and other therapeutic functionality will be maintained. This could work as a replacement/addition for other methods of myeloablation such as antibody drug conjugates.

Gene expression will be extremely important in future preclinical work, although this has been investigated more extensively than some of the other more system specific items on this list and will likely not function in different ways in either the CD90 targeting or Co-LOCKR targeting we are performing here. Implementing the Kiem Labs established systems for studying and treating Sickle Cell Disease through fetal hemoglobin reactivation would be an excellent starting point in this portion of the investigation. This would necessitate moving into non-human primates to take advantage of their more similar genetics to humans, something the Kiem lab is uniquely set up to answer with its experience working with non-human primates. Additionally, the groundworks for using the Co-LOCKR targeting to create CAR T cells in vivo is already being laid, and will partially address this question, with one possible longer-term goal of moving to making CAR T cells via HSC editing instead of direct T cell editing[77].

It is not yet fully known if the Co-LOCKR proteins will be immunogenic, and if so, the uncovering of the portion of the protein that causes immunogenicity and reordering of the protein structure to avoid such affects will be necessary. The Baker lab is uniquely suited to ensuring this process runs smoothly. In addition, the other potential immune responses, such as neutralizing antibodies against portions of the lentivirus like the measles hemagglutinin, can

be abrogated by swapping to other even more antibody avoidant proteins, such as the Cocal virus's surface proteins, which we are currently exploring its abilities to link various targeting moieties too[71, 78].

Producing more concentrated viruses that contain even higher amounts of loaded, infection competent, particles to overcome the body's ability to neutralize viruses with antibodies or other immune pathways is a problem that can hopefully be optimized in systematic, rational, and high throughput ways. Varying individual portions of the virus production protocol, as well as keeping abreast of new breakthroughs in cellular virus production schemes, can hopefully continue to improve transduction rates *in vivo*. And finally, the Kiem lab is also extremely interested in using polymeric nanoparticles as delivery agents for transient cas9 expression, as an alternative to virus gene insertion. The system we use for polymeric nanoparticle formulation is amenable to both the addition of the CD90 scFv targeting as well as any targeting ligands selected in the Co-LOCKR proteins, and experiments are ongoing to incorporate what we have found in this study into the realm of nanoparticles.

In summary, while many challenges remain, all are approachable. I hope this work can be picked up and carried forward across these many possible paths that will lead it closer to being utilized in clinical settings.

REFERENCES

1. Tang, R. and Z. Xu, *Gene therapy: a double-edged sword with great powers.* Mol Cell Biochem, 2020. **474**(1-2): p. 73-81.
2. Raguram, A., S. Banskota, and D.R. Liu, *Therapeutic in vivo delivery of gene editing agents.* Cell, 2022. **185**(15): p. 2806-2827.
3. Newby, G.A. and D.R. Liu, *In vivo somatic cell base editing and prime editing.* Mol Ther, 2021. **29**(11): p. 3107-3124.
4. Morgan, R.A., et al., *Hematopoietic Stem Cell Gene Therapy: Progress and Lessons Learned.* Cell Stem Cell, 2017. **21**(5): p. 574-590.
5. Naldini, L., *Gene therapy returns to centre stage.* Nature, 2015. **526**(7573): p. 351-60.
6. Rotin, L.E., et al., *Allogeneic Hematopoietic Stem Cell Transplant Versus Gene Therapy in Sickle Cell Disease: A Systematic Review.* Blood, 2019. **134**(Supplement_1): p. 4714-4714.
7. Peterson, C.W., et al., *Multilineage polyclonal engraftment of Cal-1 gene-modified cells and in vivo selection after SHIV infection in a nonhuman primate model of AIDS.* Mol Ther Methods Clin Dev, 2016. **3**: p. 16007.
8. Peterson, C.W., et al., *Long-term multilineage engraftment of autologous genome-edited hematopoietic stem cells in nonhuman primates.* Blood, 2016. **127**(20): p. 2416-26.
9. Wang, J., et al., *Homology-driven genome editing in hematopoietic stem and progenitor cells using ZFN mRNA and AAV6 donors.* Nat Biotechnol, 2015. **33**(12): p. 1256-1263.
10. Genovese, P., et al., *Targeted genome editing in human repopulating haematopoietic stem cells.* Nature, 2014. **510**(7504): p. 235-240.
11. Baldo, A., et al., *General considerations on the biosafety of virus-derived vectors used in gene therapy and vaccination.* Curr Gene Ther, 2013. **13**(6): p. 385-94.
12. Raper, S.E., et al., *Fatal systemic inflammatory response syndrome in a ornithine transcarbamylase deficient patient following adenoviral gene transfer.* Mol Genet Metab, 2003. **80**(1-2): p. 148-58.
13. Hacein-Bey-Abina, S., et al., *LMO2-associated clonal T cell proliferation in two patients after gene therapy for SCID-X1.* Science, 2003. **302**(5644): p. 415-9.
14. Stein, S., et al., *Genomic instability and myelodysplasia with monosomy 7 consequent to EVI1 activation after gene therapy for chronic granulomatous disease.* Nat Med, 2010. **16**(2): p. 198-204.
15. Braun, C.J., et al., *Gene therapy for Wiskott-Aldrich syndrome--long-term efficacy and genotoxicity.* Sci Transl Med, 2014. **6**(227): p. 227ra33.
16. Braun, C.J., et al., *Gene therapy for Wiskott-Aldrich Syndrome-Long-term reconstitution and clinical benefits, but increased risk for leukemogenesis.* Rare Dis, 2014. **2**(1): p. e947749.
17. Morrison, C., *$1-million price tag set for Glybera gene therapy.* Nat Biotechnol, 2015. **33**(3): p. 217-8.
18. Melchiorri, D., et al., *Regulatory evaluation of Glybera in Europe - two committees, one mission.* Nat Rev Drug Discov, 2013. **12**(9): p. 719.
19. Staal, F.J.T., A. Aiuti, and M. Cavazzana, *Autologous Stem-Cell-Based Gene Therapy for Inherited Disorders: State of the Art and Perspectives.* Front Pediatr, 2019. **7**: p. 443.
20. Río, P., S. Navarro, and J.A. Bueren, *Advances in Gene Therapy for Fanconi Anemia.* Hum Gene Ther, 2018. **29**(10): p. 1114-1123.

21. Wu, J., et al., *Liposome-mediated extracellular superoxide dismutase gene delivery protects against acute liver injury in mice.* Hepatology, 2004. **40**(1): p. 195-204.
22. Wei, T., et al., *Systemic nanoparticle delivery of CRISPR-Cas9 ribonucleoproteins for effective tissue specific genome editing.* Nat Commun, 2020. **11**(1): p. 3232.
23. Majeti, R., C.Y. Park, and I.L. Weissman, *Identification of a hierarchy of multipotent hematopoietic progenitors in human cord blood.* Cell Stem Cell, 2007. **1**(6): p. 635-45.
24. Benedict, C.A., et al., *Targeting retroviral vectors to CD34-expressing cells: binding to CD34 does not catalyze virus-cell fusion.* Hum Gene Ther, 1999. **10**(4): p. 545-57.
25. Radtke, S., et al., *Purification of Human CD34(+)CD90(+) HSCs Reduces Target Cell Population and Improves Lentiviral Transduction for Gene Therapy.* Mol Ther Methods Clin Dev, 2020. **18**: p. 679-691.
26. Brendel, C., et al., *CD133-targeted gene transfer into long-term repopulating hematopoietic stem cells.* Mol Ther, 2015. **23**(1): p. 63-70.
27. Görgens, A., et al., *New relationships of human hematopoietic lineages facilitate detection of multipotent hematopoietic stem and progenitor cells.* Cell Cycle, 2013. **12**(22): p. 3478-82.
28. Wisniewski, D., et al., *Further phenotypic characterization of the primitive lineage-CD34+CD38-CD90+CD45RA- hematopoietic stem cell/progenitor cell sub-population isolated from cord blood, mobilized peripheral blood and patients with chronic myelogenous leukemia.* Blood Cancer J, 2011. **1**(9): p. e36.
29. Basner-Tschakarjan, E. and F. Mingozzi, *Cell-Mediated Immunity to AAV Vectors, Evolving Concepts and Potential Solutions.* Front Immunol, 2014. **5**: p. 350.
30. Sauzay, C., et al., *CD90/Thy-1, a Cancer-Associated Cell Surface Signaling Molecule.* Front Cell Dev Biol, 2019. **7**: p. 66.
31. Li, Q., et al., *THY-1 cell surface antigen (CD90) has an important role in the initial stage of human cytomegalovirus infection.* PLoS Pathog, 2015. **11**(7): p. e1004999.
32. Li, Q., E. Fischer, and J.I. Cohen, *Cell Surface THY-1 Contributes to Human Cytomegalovirus Entry via a Macropinocytosis-Like Process.* J Virol, 2016. **90**(21): p. 9766-9781.
33. Radtke, S., et al., *MISTRG mice support engraftment and assessment of nonhuman primate hematopoietic stem and progenitor cells.* Exp Hematol, 2019. **70**: p. 31-41.e1.
34. Radtke, S., et al., *A distinct hematopoietic stem cell population for rapid multilineage engraftment in nonhuman primates.* Sci Transl Med, 2017. **9**(414).
35. Masiuk, K.E., et al., *Improving Gene Therapy Efficiency through the Enrichment of Human Hematopoietic Stem Cells.* Mol Ther, 2017. **25**(9): p. 2163-2175.
36. Zonari, E., et al., *Efficient Ex Vivo Engineering and Expansion of Highly Purified Human Hematopoietic Stem and Progenitor Cell Populations for Gene Therapy.* Stem Cell Reports, 2017. **8**(4): p. 977-990.
37. Gordon, P.R., et al., *Large-scale isolation of CD133+ progenitor cells from G-CSF mobilized peripheral blood stem cells.* Bone Marrow Transplant, 2003. **31**(1): p. 17-22.
38. Moraes, D.A., et al., *A reduction in CD90 (THY-1) expression results in increased differentiation of mesenchymal stromal cells.* Stem Cell Res Ther, 2016. **7**(1): p. 97.
39. Kumar, A., et al., *Multiple roles of CD90 in cancer.* Tumour Biol, 2016. **37**(9): p. 11611-11622.
40. Kirkpatrick, R.L., et al., *Conditional Recruitment to a DNA-Bound CRISPR-Cas Complex Using a Colocalization-Dependent Protein Switch.* ACS Synth Biol, 2020. **9**(9): p. 2316-2323.
41. Lajoie, M.J., et al., *Designed protein logic to target cells with precise combinations of surface antigens.* Science, 2020. **369**(6511): p. 1637-1643.
42. Brendel, C., et al., *CD133-targeted gene transfer into long-term repopulating hematopoietic stem cells.* Mol Ther, 2015. **23**(1): p. 63-70.

43. Gorgens, A., et al., *Revision of the human hematopoietic tree: granulocyte subtypes derive from distinct hematopoietic lineages.* Cell Rep, 2013. **3**(5): p. 1539-52.
44. Radtke, S., et al., *CD133 allows elaborated discrimination and quantification of haematopoietic progenitor subsets in human haematopoietic stem cell transplants.* Br J Haematol, 2015. **169**(6): p. 868-78.
45. Humbert, O., et al., *Therapeutically relevant engraftment of a CRISPR-Cas9-edited HSC-enriched population with HbF reactivation in nonhuman primates.* Sci Transl Med, 2019. **11**(503).
46. Craig, W., et al., *Expression of Thy-1 on human hematopoietic cells.* Journal of Experimental Medicine, 1993. **177**: p. 1331-1342.
47. von Boehmer, L., et al., *Sequencing and cloning of antigen-specific antibodies from mouse memory B cells.* Nat Protoc, 2016. **11**(10): p. 1908-1923.
48. Lefranc, M.P., et al., *IMGT(R), the international ImMunoGeneTics information system(R) 25 years on.* Nucleic Acids Res, 2015. **43**(Database issue): p. D413-22.
49. Lefranc, M.P., *Immunoglobulin and T Cell Receptor Genes: IMGT((R)) and the Birth and Rise of Immunoinformatics.* Front Immunol, 2014. **5**: p. 22.
50. Grosdidier, A., V. Zoete, and O. Michielin, *SwissDock, a protein-small molecule docking web service based on EADock DSS.* Nucleic Acids Res, 2011. **39**(Web Server issue): p. W270-7.
51. Dunbar, J., et al., *SAbPred: a structure-based antibody prediction server.* Nucleic Acids Res, 2016. **44**(W1): p. W474-8.
52. Anliker, B., et al., *Specific gene transfer to neurons, endothelial cells and hematopoietic progenitors with lentiviral vectors.* Nat Methods, 2010. **7**(11): p. 929-35.
53. Levy, C., et al., *Measles virus envelope pseudotyped lentiviral vectors transduce quiescent human HSCs at an efficiency without precedent.* Blood Adv, 2017. **1**(23): p. 2088-2104.
54. Frecha, C., et al., *Stable transduction of quiescent T cells without induction of cycle progression by a novel lentiviral vector pseudotyped with measles virus glycoproteins.* Blood, 2008. **112**(13): p. 4843-52.
55. Funke, S., et al., *Targeted cell entry of lentiviral vectors.* Mol Ther, 2008. **16**(8): p. 1427-36.
56. Bandaranayake, A.D., et al., *Daedalus: a robust, turnkey platform for rapid production of decigram quantities of active recombinant proteins in human cell lines using novel lentiviral vectors.* Nucleic Acids Res, 2011. **39**(21): p. e143.
57. Kedmi, R., et al., *A modular platform for targeted RNAi therapeutics.* Nat Nanotechnol, 2018. **13**(3): p. 214-219.
58. De, B.P., et al., *In Vivo Potency Assay for Adeno-Associated Virus-Based Gene Therapy Vectors Using AAVrh.10 as an Example.* Hum Gene Ther Methods, 2018. **29**(3): p. 146-155.
59. van Haasteren, J., S.C. Hyde, and D.R. Gill, *Lessons learned from lung and liver in-vivo gene therapy: implications for the future.* Expert Opin Biol Ther, 2018. **18**(9): p. 959-972.
60. Kleinlutzum, D., et al., *Enhancing the oncolytic activity of CD133-targeted measles virus: Receptor extension or chimerism with vesicular stomatitis virus are most effective.* Front Oncol, 2017. **7**: p. 127.
61. Niu, F., et al., *Lanthanide-doped nanoparticles conjugated with an anti-CD33 antibody and a p53-activating peptide for acute myeloid leukemia therapy.* Biomaterials, 2018. **167**: p. 132-142.
62. Rosenblum, D., et al., *CRISPR-Cas9 genome editing using targeted lipid nanoparticles for cancer therapy.* Sci Adv, 2020. **6**(47).
63. Zheng, Y., et al., *In vivo targeting of adoptively transferred T-cells with antibody- and cytokine-conjugated liposomes.* Journal of Controlled Release, 2013. **172**(2): p. 426-435.

64. Kneissl, S., et al., *Measles virus glycoprotein-based lentiviral targeting vectors that avoid neutralizing antibodies.* PLoS One, 2012. **7**(10): p. e46667.
65. Moffett, H.F., et al., *Hit-and-run programming of therapeutic cytoreagents using mRNA nanocarriers.* Nat Commun, 2017. **8**(1): p. 389.
66. Veiga, N., et al., *Cell specific delivery of modified mRNA expressing therapeutic proteins to leukocytes.* Nat Commun, 2018. **9**(1): p. 4493.
67. Rudnicka, D., et al., *Simultaneous cell-to-cell transmission of human immunodeficiency virus to multiple targets through polysynapses.* J Virol, 2009. **83**(12): p. 6234-6246.
68. Yang, R., et al., *Effective elimination of liver cancer stem-like cells by CD90 antibody targeted thermosensitive magnetoliposomes.* Oncotarget, 2016. **7**(24): p. 35894-35916.
69. Adair, J.E., et al., *Semi-automated closed system manufacturing of lentivirus gene-modified haematopoietic stem cells for gene therapy.* Nat Commun, 2016. **7**: p. 13173.
70. Rajawat, Y.S., et al., *In Vivo Gene Therapy for Canine SCID-X1 Using Cocal-Pseudotyped Lentiviral Vector.* Hum Gene Ther, 2021. **32**(1-2): p. 113-127.
71. Trobridge, G.D., et al., *Cocal-pseudotyped lentiviral vectors resist inactivation by human serum and efficiently transduce primate hematopoietic repopulating cells.* Mol Ther, 2010. **18**(4): p. 725-33.
72. El Kharrag, R.B., K.; Madhu, R.; Cui, M.; Campoy, G.; Mack, H.; Wolf, C.; Perez, A.; Humbert, O.; Kiem HP.; Radtke, S., *Efficient polymer nanoparticle-mediated delivery of gene editing reagents into human hematopoietic stem and progenitor cells.* Molecular Therapy, 2022. **(in revision)**.
73. Banskota, S., et al., *Engineered virus-like particles for efficient in vivo delivery of therapeutic proteins.* Cell, 2022. **185**(2): p. 250-265 e16.
74. Anliker, B., et al., *Specific gene transfer to neurons, endothelial cells and hematopoietic progenitors with lentiviral vectors.* Nat Methods, 2010. **7**(11): p. 929-35.
75. Dobson, C.S., et al., *Antigen identification and high-throughput interaction mapping by reprogramming viral entry.* Nat Methods, 2022. **19**(4): p. 449-460.
76. Pan, D., et al., *Biodistribution and toxicity studies of VSVG-pseudotyped lentiviral vector after intravenous administration in mice with the observation of in vivo transduction of bone marrow.* Mol Ther, 2002. **6**(1): p. 19-29.
77. Haworth, K.G., et al., *In Vivo Murine-Matured Human CD3.* Mol Ther Methods Clin Dev, 2017. **6**: p. 17-30.
78. Humbert, O., et al., *Development of Third-generation Cocal Envelope Producer Cell Lines for Robust Lentiviral Gene Transfer into Hematopoietic Stem Cells and T-cells.* Mol Ther, 2016. **24**(7): p. 1237-46.
79. Sun, Y., et al., *Degenerate primer design to clone the human repertoire of immunoglobulin heavy chain variable regions.* World J Microbiol Biotechnol, 2012. **28**(1): p. 381-6.

MATERIALS AND METHODS

mRNA extraction, cDNA synthesis, and heavy/light chain sequencing of the hybridoma cells

mRNA was extracted from the hybridoma cells using an RNAeasy kit (Qiagen USA, MD). Extracted mRNA was run on tapestation (Aligent USA, CA) for integrity. cDNA was generated from mRNA using an applied biosystem high capacity RNA-to-cDNA kit (Thermofisher, USA, MA). Primers for the variant regions of the antibody were acquired from the literature [79] and ordered using IDT. CD90 ab internal reverse primer (TTC AGT CAC CAT GCT GTT GAC) forward primer (CCA GCA GAA GCC AGG ATC). Antibody variable regions were sequenced using on an Applied Biosystems 3730xl DNA Analyzers (Thermo Fisher, USA, MA)). Raw

sequencing data was analyzed using International ImMunoGeneTics V-QUEry and STandardization program to align and annotate the antibody sequence.

Modeling and Visualization of Proteins:

The antibody structure was predicted with SabPred [51]. Antibody-protein docking was predicted using Swissdock [50]. Visualizations were generated with Pymol (*The PyMOL Molecular Graphics System, Version 2.0 Schrödinger, LLC*).

Cloning of Virus Plasmids:

Measles plasmid were provided by Els Verhoeyen [53]. Cloning was performed using restriction enzymes from New England Biosciences (USA) and Gibson Assembly Master Mix (NEB, USA). DNA tiles containing the desired sequences to be cloned into the plasmids were acquired from Codex DNA (Codex DNA, USA, CA). Cloned products were confirmed via sequencing on an Applied Biosystems 3730xl DNA Analyzers (Thermo Fisher, USA, MA). The relevant sequences are in **Supplemental Figure 1**.

VSVG Knockout (KO) and Targeted binder plasmids were provided by the Baker Laboratory (Institute of Protein Design, University of Washington, Seattle, WA). Cloning of BCL-2 Targeting ligand into the targeted binder plasmid was performed by Eco721-FastDigest (ThermoFisher, cat # FD0364) and Eco1471-FastDigest (ThermoFisher, cat # FD0424) restriction enzyme digest of targeted binder plasmid followed by Gibson Assembly (New England Bioscience, cat # E2611S) with synthesized DNA Tiles (Codex DNA, CA, USA) containing the BCL-2 sequence. Successful cloning was confirmed by EcoRI (New England Biosciences, cat # R3101S) restriction enzyme

digest, followed by sequencing on Applied Biosystems 373xl DNA Analyzers (Thermo Fisher, MA, USA).

Virus production

HEK293T cells were expanded on gelatin coated plates and transfected with plasmids mixed with PEI (Polysciences, USA, PA) at a ¼ ug plasmid to ug PEI ratio. Measles virus plasmid ratios were 27ug pLenti-EF1a-mScarlet-I-WPRE transfer plasmid, 17ug 2nd generation Gag/Pol Helper plasmid pCMVdelta8.74, 10ug measles hemagglutinin Delta 24H or other relevant targeting ligand, and 10ug measles fusion Delta F per 15cm cell plate. VSVG virus plasmid ratios were 27ug pLenti-EF1a-mScarlet-I-WPRE transfer, 17ug second generation Gag/Pol Helper plasmid pCMVdelta8.74, 10ug VSVG fusion, and 10ug of relevant targeting ligand plasmid per 15cm cell plate. 24 hours after transfection, the media was changed to LV-MAX (Thermofisher, USA, MA) media with 20mM HEPES (Thermofisher, USA, MA) and 1X L-glutamine (Thermofisher, USA, MA). Virus production media was allowed to sit for a further 24 hours, then the supernatant was collected, spun down at 800g to remove cellular debris, filtered with an 8um filter, and spun down for 24 hours at 4800g. The concentrated supernatant was resuspended at a 1/100 volume.

Hydrodynamic titration

Hydrodynamic titration of viral particles was performed on a Zetaviewer machine (Particle Metrix Germany). The machine was calibrated with a 100nm bead test sample prior to all measurements. Viruses were diluted 1 to 1000 in molecular grade water and analyzed for their size characteristics. Readouts from the machine were back calculated to account for dilution. Diluted virus samples were next incubated with 1x SYBR II Green RNA stain (Thermofisher, United States, MA) for 5

minutes before running on the Zetaviewer with a 488 nm filter in place to only identify virus particles loaded with mRNA and stained with SYBR II. Additionally, virus's targeted to CD90 were incubated with SYBR II and CD90-mCherry protein for 30 minutes. Viruses targeted to BIM were incubated with SYBR II and BIM-HER2-mCherry protein for 30 minutes prior to size analysis. Virus-protein complexes were analyzed on the Zetaviewer with a 488 or 520 nm filter in place to capture particles loaded with mRNA carrying CD90-mCherry.

CD90 Fab Production

Anti-CD90 IgGs were produced by the Antibody Technology Core at the Fred Hutchinson Cancer Center from the previously reported hybridoma cell lines producing the CD90 antibody clone 5E10 [46]. Fab fragments were generated from full-length CD90 antibodies with immobilized papain (Thermo Scientific Cat. Number 20341) per manufacture protocol. After verifying full digestion by SDSPAGE, the reaction mixture was buffer exchanged into PBS and the Fab separated from the Fc by anion exchange chromatography using a HiTrap Q column on an ÄKTA Pure.

CD90-mCherry Production

The CD90-mCherry Fusion protein was expressed in HEK293 cells as the following amino acid sequence:

```
1 METDT LLLWV LLLWV PGSTG QKVTS LTACL VDQSL RLDCR HENTS SSPIQ
51   YEFSL TRETK KHVLF GTVGV PEHTY RSRTN FTSKY NMKVL YLSAF TSKDE
101  GTYTC ALHHS GHSPP ISSQN VTVLR DKLVK CEGGS GGGSG GGVSK GEEDN
151  MAIIK EFMRF KVHME GSVNG HEFEI EGEGE GRPYE GTQTA KLKVT KGGPL
201  PFAWD ILSPQ FMYGS KAYVK HPADI PDYLK LSFPE GFKWE RVMNF EDGGV
251  VTVTQ DSSLQ DGEFI YKVKL RGTNF PSDGP VMQKK TMGWE ASSER MYPED
```

301 GALKG EIKQR LKLKD GGHYD AEVKT TYKAK KPVQL PGAYN VNIKL DITSH

351 NEDYT IVEQY ERAEG RHSTG GMDEL YK*

Sequence Nomenclature	Coloring Schema	Sequence Numbering
Protein Release Ladder		1-20
CD90 protein		21-133
Linker		134-142
mCherry		143-377

The DNA was codon optimized for human expression, cloned into a modified lentivirus expression system, and expressed as described in [56]. The media containing the secreted CD90-mCherry was concentrated and purified using a P200 SEC column equilibrated in PBS buffer.

Cell Lines

Jurkat (ATCC CLR-2899) cells, K562(ATCC CCL-243 and Raji (ATCC CCL-86) cells were cultured in RPMI with Penicillin Streptomycin at a final concentration of 50 to 100 I.U./mL (ThermoFisher Scientific) and supplemented with 10% cosmic calf serum (ThermoFisher Scientific).

Primary human HSCs

Primary human $CD34^+$ cells were purchased from the Co-operative Center for Excellence in Hematology (CCEH) at the Fred Hutchinson Cancer Research Center. Collections were performed according to the Declaration of Helsinki and were approved by a local ethics committee/institutional review board of the Fred Hutchinson Cancer Research Center. All healthy adult donors were mobilized with GCSF. Human $CD34^+$ cells were enriched as previously

described on a CliniMACS Prodigy according to the manufacturer's instructions (Miltenyi Biotec, Bergisch Gladbach, Germany).

Human $CD34^+$ cells were cultured in StemSpan (STEMCELL Technologies, Vancouver, BC, Canada) medium supplemented with penicillin-streptomycin (PS) (100 U/mL) (Gibco by Life Technologies, Waltham, MA, USA) and 100 ng/mL of each stem cell factor (PeproTech, Cranbury, NJ, USA), thrombopoietin (TPO; PeproTech), and Fms-related tyrosine kinase 3 ligand (FLT3-L; Miltenyi Biotec). Cells were cultured at 37°C, 85% relative humidity, and 5% CO2.

Virus Transduction

Cells (Jurkat, Raji, human HSCs) were resuspended in serum free media at a density of 150,000 cells per 150 μL per well of a 96 well plate (Corning, Corning, NY, USA). Concentrated viral supernatant was added to the cells, and in case of Co-LOCKR experiments, relevant proteins were added immediately after addition of virus. Afterward cells were incubated for 8-12 hours. Multiplicity of infection and desired transduction rate were back calculated from the hydrodynamic titer obtained for the specific virus batch being used. After transduction cells were washed and media replaced with relevant growth media specific to cell type (see above). In Co-LOCKR experiments, viruses and proteins were incubated with cells at the same time and washed after 8-12 hours and replaced with fresh media. Transgene expression was determined flow-cytometrically 72-120 hours post-transduction.

Viability assessment and counting of human $CD34^+$ cells and cells lines.

The cell viability was analyzed using the Countess II FL automated cell counter (Thermo Fisher Scientific). A 10 μL volume of trypan blue stain (0.4%) (Invitrogen, Waltham, MA, USA) was mixed with 10 μL of cell suspension, and 10 μL of the mixture was applied to a disposable cell counting chamber slide and inserted into the device. The percentage of cell viability for each sample was recorded in duplicate and reported as the mean ± SEM.

Flow cytometry analysis and cell sorting

Flow cytometric analysis and sorting of cell lines and human $CD34^+$ cells were performed using the fluorochrome-conjugated antibodies listed in **Supplemental Table 1**. Dead cells and debris were excluded via forward light scatter (FSC)/side light scatter (SSC) gating and DAPI staining. Flow cytometric analysis and cell sorting were performed on a FACSymphony A5, FACSCelesta, FACSAria IIu, and Symphony S6 (BD Biosciences). Data were acquired using FACSDiva version 6.1.3 and newer (BD Biosciences). Data analysis was performed using FlowJo version 8 and higher (BD Biosciences).

CFC assay

For CFC assays, 200 FACS-purified $CD34^+mScarlet^+$ cells were seeded on 30 mm plates in 1 mL of methylcellulose (MethoCult H4435, STEMCELL Technologies). Colonies were counted and scored after 12–14 days according to morphology into colony-forming unit (CFU)-granulocyte (CFU-G), CFU-macrophage (CFU-M), granulocyte-macrophage (CFU-GM), and burst-forming unit-erythrocyte (BFU-E). Colonies consisting of erythroid and myeloid cells were scored as CFU-Mix. For secondary CFC assays, primary colonies were harvested, washed twice with PBS, and

5% of cell suspension replated into 1 mL of methylcellulose. Secondary colonies were counted and scored after 12–14 days.

Protein Enhancements:

Co-LOCKR modification and enhancements were performed by the Baker lab.

Co-LOCKR protein production and purification was performed by the Baker lab.

Mouse Transplantation and In Vivo Editing

For the in vivo targeting of Raji Cells, Adult (8-12) week NSG or NSGW mice were irradiated at 275 cGy. 4 hours later the mice were injected with either 200ul of Raji cells via tail vein or 15ul of Raji cells via intra-bone marrow injection. 3 days later mice were injected with virus and Co-LOCKR components 200ul via tail vein or 15ul via intra-bone marrow injection. All animal studies were carried out at the Fred Hutchinson Cancer Research Center in compliance with the approved Institutional Animal Care and Use Committee (IACUC) protocol 1483.

Statistical Analysis

All figures and statistical analysis were performed/designed with Prism Software.

Biorender was used in the construction of some figures.

"Go on, get out! Last words are for fools who haven't said enough!"